Title: Advances in Ground Improvement Using Waste Materials for Transportation Infrastructure

Authors:

***Buddhima Indraratna**

PhD, FTSE, FIEAust, FASCE, FGS, Distinguished Professor, Founding Director of Center for Geomechanics and Railway Engineering (CGRE), Director of Australian Research Council's National Training Centre for Advanced Technologies in Rail Track Infrastructure (ITTC-Rail), University of Wollongong, NSW 2522, Australia. https://orcid.org/0000-0002-9057-1514

Yujie Qi

PhD, AMASCE, Associate Research Fellow, Centre for Geomechanics and Railway Engineering, University of Wollongong, Wollongong, Australia, https://orcid.org/0000-0002-3486-2130

Miriam Tawk

PhD Candidate, Centre for Geomechanics and Railway Engineering, University of Wollongong, Wollongong, Australia, https://orcid.org/0000-0002-1317-6297

Ana Heitor

PhD, MIEAust, Lecturer, School of Civil Engineering, University of Leeds, Leeds, UK, https://orcid.org/0000-0002-2346-8250

Cholachat Rujikiatkamjorn

PhD, Associate Professor, Centre for Geomechanics and Railway Engineering, Australian Research Council's National Training Centre for Advanced Technologies in Rail Track Infrastructure (ITTC-Rail), University of Wollongong, Wollongong, Australia, https://orcid.org/0000-0001-8625-2839

Sinniah K. Navaratnarajah

PhD, Senior Lecturer and Lecturer In-Charge of Geotechnical Laboratory, Department of Civil Engineering, Faculty of Engineering, University of Peradeniya, Peradeniya, Sri Lanka, https://orcid.org/0000-0002-7936-520X

***Author for correspondence:**
Distinguished Prof. Buddhima Indraratna
School of Civil, Mining & Environmental Engineering,
Faculty of Engineering and Information Science,
University of Wollongong Australia
Wollongong, NSW 2522, AUSTRALIA
Ph: +61 2 4221 3046，Fax: +61 2 4221 3238，Email: indra@uow.edu.au

Abstract: Recycling waste materials for transport infrastructure such as coal wash (CW), steel furnace slag (SFS), fly ash (FA) and recycled tyre products is an efficient way of minimising the stockpiles of waste materials while offering significant economic and environmental benefits, as well as improving the stability and longevity of infrastructure foundations. This paper presents some of the most recent state-of-the-art studies undertaken at the University of Wollongong Australia on the use of waste materials such as, (i) CW-based granular mixtures (i.e. SFS+CW, CW+FA) for port reclamation and road base/subbase, and (ii) using recycled tyre products (i.e. rubber crumbs, tyre cell, under sleeper pads and under ballast mats) to increase track stability and reduce ballast degradation. Typical methods of applying these waste materials for different infrastructure conditions are described and the results of comprehensive laboratory and field tests are presented and discussed.

Keywords: Recycling and reuse of materials, Geotechnical engineering, granular materials, railway tracks

1. Introduction

Stockpiling mining waste has created serious environmental and social concerns for many mining-based countries such as Australia. Steel furnace slag (SFS) and coal wash (CW) are two common granular by-products from steel manufactures and coal mining, and every year millions of tonnes are produced in Australia; most is stockpiled, while the recycling rate barely meets satisfactory (Mudd, 2010). Furthermore, since good quality natural aggregates are becoming increasingly scarce and associated environmental legislation becoming more stringent, finding sustainable and innovative ways of recycling various types of industry wastes (used tyre derivatives, coal wash, plastics, glass etc.) for developing civil infrastructure will become crucial (Indraratna *et al.*, 2018; Indraratna *et al.*, 2019a; Arulrajah *et al.*, 2020a; Arulrajah *et al.*, 2020b; Naeini *et al.*, 2020; Suddeepong *et al.*, 2020). The commercial use of these engineered fills (SFS and CW) above the groundwater level has already been approved by the Environment Protection Authority of the state of New South Wales (NSW EPA, 2014ab) indicating insignificant leachate potential and toxicity. Humphrey et al. (1997), Edil and Bossscher (1992), and Downs et al. (1996) carried out field studies of shredded rubber above and below the water table and they found insignificant leaching of hazardous compounds, i.e. even below the typical limits in drinking water standards

SFS is produced when converting iron to steel through a basic oxygen furnace and CW is generated while separating coal from its impurities. Apart from CW, fly ash (FA) is another by-product from coal that is generated when burning coal in electric generation power plants. FA contains some materials like aluminous and siliceous that form cement with chemical reaction with water, and this material is usually considered to be a stabilising agent for base and subbase materials (Ahmaruzzaman, 2010; Wang *et al.*, 2019). While SFS particles have a higher unit weight and superior shear strength and stiffness than natural aggregates (Wang, 2010; Yildirim and Prezzi, 2015; Qi *et al.*, 2018a); previous studies (e.g. Indraratna, 1994; Heitor *et al.*, 2016; Fityus *et al.*, 2008) reported that coal wash is suitable for structural fill based on its shear strength, and the impact of breakage (during compaction and shearing) and associated double porosity in its compacted state can affect its shear and deformation behaviour significantly (i.e. Rujikiatkamjorn *et al.*, 2013; Kaliboullah *et al.* 2015). However, improving heterogeneous waste materials such as SFS and CW through compaction poses some challenges related to their individual adverse geotechnical properties, i.e. the breakage potential for coal wash (Indraratna, 1994; Heitor *et al.*, 2016) and volumetric instability (swelling) for steel furnace slag (Wang, 2010; Heitor *et al.*, 2014). To minimise these detrimental effects and optimise the geotechnical properties, these waste materials are usually blended with other materials before using them for civil engineering applications. For instance, SFS can be blended with fly ash, cement, asphalt or concrete to serve as a landfill or a pavement material (Xue *et al.*, 2006; Malasavage *et al.*, 2012; Yildirim and Prezzi, 2015), CW is mixed with FA and then used as alternative aggregates for base and subbase materials in roads (Wang *et al.*, 2019), and it has been reported that SFS and CW blended in a proper ratio can successfully serve as construction fill in port and land reclamation projects (Indraratna *et al.*, 1994; Heitor *et al.*, 2014; Chiaro *et al.*, 2015; Tasalloti *et al.*, 2015a, b).

The accumulation of waste tyres is another concern for most developed and developing countries; in Australia alone, more than 50 million (Equivalent Passenger Unit) waste tyres are generated every year (Brulliard *et al.*, 2012). To tackle the problem of large stockpiles of waste tires, researchers have proposed innovative ways to reuse waste tire products in civil engineering, especially transport infrastructure projects such as railways, highways, and seismic isolation. This is because the high damping property and high energy absorbing capacity of rubber help to attenuate dynamic loads and vibrations and hence reduce the degradation of infrastructure foundations and enhance stability and longevity (Schneider *et al.*, 2011; Costa

et al., 2012; Sol-Sánchez *et al.*, 2015; Indraratna *et al.*, 2018; Qi *et al.*, 2018c; Indraratna *et al.*, 2019a). Several types of recycled rubber products have been introduced into railway, i.e. under sleeper pads (USP), under ballast mats (UBM), recycled tyre cells and granulated rubber/rubber crumbs (Nimbalkar and Indraratna, 2016; Indraratna *et al.*, 2017a; Indraratna *et al.*, 2017b; Indraratna *et al.*, 2017c; Navaratnarajah and Indraratna, 2017; Indraratna *et al.*, 2018; Navaratnarajah *et al.*, 2018; Indraratna *et al.*, 2019b; Jayasuriya *et al.*, 2019; Sol-Sánchez *et al.*, 2019). Furthermore, mixing rubber crumbs (RC) with mining waste (i.e. SFS, CW) can further improve the energy absorption properties of these waste mixtures and also extend the application of these mining waste into the rail foundations (Indraratna *et al.*, 2017a; Indraratna *et al.*, 2019b).

This paper reviews the recent novel studies at the University of Wollongong (Australia), on the use of waste materials (i.e. SFS, CW, FA and recycled tyre products) in port reclamation and roads and railways, these applications include (i) using blends of SFS and CW for port reclamation, (ii) evaluating a mixture of CW and FA for road base/subbases, (iii) two methods for developing a synthetic energy absorbing layer for railway subballast using mixtures of SFS+CW+RC or CW+RC, (iv) using recycled tyre cells to reinforce the capping layer for heavy haul rail tracks, and (v) using rubber mats (i.e. USP, UBM) to reduce ballast degradation and track deformation under stiff subgrade conditions such as tunnels and bridges. Comprehensive laboratory tests (small scale and large scale) were carried out to investigate the geotechnical properties of these novel waste-material inclusions. The details of general test procedures and typical sample preparation process have been described elsewhere (e.g. Chiaro et al. 2015; Indraratna et al. 2017a), where the target material is based on optimizing the blended materials in various proportions according to the type of infrastructure and the nature of loading anticipated. These research outcomes are expected to contribute to better design solutions where recycled materials are used to enhance the stability and longevity of infrastructure, while simultaneously reducing the number and volume of waste stockpiles and the demand for natural aggregates.

2. Coal Wash-Based Waste Granular Materials for Roads and Port Reclamation

2.1 Compacted CW with blends of SFS for port infrastructure

2.1.1 Materials

Using locally available granular waste materials such as coal wash (CW) and steel furnace slag (SFS) for reclamation fills in port infrastructure is an economical alternative to conventional (quarried) aggregates and dredged sandy fills. CW is a by-product from the washery process for refining run-of-mine (ROM) coal. For every metric tonne of ROM coal that enters a washery plant, approximately 200kg of the output are granular waste materials, of which 80% corresponds to coarse-grained coal wash and 20% are fine-grained tailings. Coal mining operations in Australia alone generate millions of tonnes per year of CW (Chiaro et al., 2015). SFS by-product is a direct result of steelmaking as iron and steel scrap are processed with lime at high temperatures in Basic Oxygen (BOF) and Electric Arc (EAF) furnaces. Approximately 10-15% of the output by weight from a BOF is SFS. In this study, the source CW (specific gravity $G_s = 2.27$) is Dendrobium CW produced by Illawarra Coal, and the SFS ($G_s = 3.34$) is produced via the basic oxygen method at Australia Steel Milling Services. Their particle size distribution curves are given in Figure 1.

2.1.2 Applications in Port conditions and results of field trials

The typical specifications of fill materials for Port conditions rely on characterising the material in terms of its shear strength (i.e. peak friction angle, $\phi'_{peak} > 30°$) and permeability (between 1×10^{-6} cm/s and 1×10^{-4} cm/s, (Davies *et al.*, 2011)). However, for the CW and CW+SFS blends, additional parameters such as the breakage potential and swelling must be considered. While compacted coal wash can easily exceed the required peak friction angle of 30°, it still exhibits excessive breakage during shearing. This is very evident when the stress levels are higher than the critical breakage stress of 127 kPa (Heitor *et al,* 2016), and this is why Chiaro *et al.* (2015) proposed a modified criteria for selecting an optimal CW+SFS blend ratio that meets the specifications established for Port conditions and complies with the allowable volumetric changes during service. The proposed criteria has four levels of acceptance, as shown in Figure 2. The region that defines the optimal mixing ratio of CW+SFS lies between 55%<CW<70%; within this range the blends can easily comply with the acceptance criteria defined for structural fill.

Once suitable CW+SFS blend ratios were identified, a field trial took place at the Port Kembla Outer Harbor reclamation site in an area 55 m long by 14 m wide by 1.4 m deep (i.e. 1078 m^3) assigned by the Port

Kembla Port Corporation. This area was then divided into two sections so that the two selected blends could be assessed. The ratios of these mixtures were based on a preliminary study conducted by Chiaro *et al.* (2015), i.e. CW50+SFS50 and CW20+SFS80 by volume percentage. The materials were mixed and placed in situ by an excavator, and then spreaded and levelled with a grader (Figure 3a). The CW+SFS blends were compacted by a 13 tonne smooth steel drum roller running on a vibration mode of 30 Hz (Figure 3b). After four to eight passes with the roller, the mixtures could attain 90% to 95% dry unit weight complying with the required specifications for port expansion (Davies et al., 2011).

Dynamic Cone Penetration Tests (DCPTs) and Plate Load Tests (PLTs) were then carried out to assess the post-compaction shear strength of these mixtures. During the DCPT tests the number of blows to drive the cone penetrometer 100 mm into the compacted layers was measured regularly (ASTM D6951, 2009); Figure 3 (c-d) shows the equivalent in-situ California Bearing Ratio (CBR) values obtained via the number of DCPT blows ($CBR = 292/DCP^{1.12}$) following ASTM D6951 (2009). Since these mixtures had an equivalent CBR value between 25 and 50, they could be considered suitable for a structural fill in terms of their shear strength.

Plate load tests for each mixture were carried out at two elapsed time periods to investigate the potential effects of the hydration reactions due to the presence of free lime (CaO) and free magnesium (MgO) in the SFS. The variation of applied pressure with settlement, for the two stages (i.e. 30 and 170 days after compaction) is shown in Figure 3 (e-f). Not surprisingly, the blend with a higher percentage of SFS (Figure 3f) had the largest difference between the 30 and 170 day tests. From the viewpoint of post-construction settlement and the expected port service loads (60-120 kPa), the expected settlement would not exceed 1 mm; this result confirmed the blend's suitability as a structural fill.

The presence of CaO and MgO in the SFS may cause the mixtures to experience swelling. To investigate the swelling potential (ratio of vertical expansion to the layer thickness), surface markers were monitored over time with surveying equipment. While the mixture with a higher SFS showed more swelling, it was still modest for a free swelling condition; the swelling potential of the CW50+SFS50 and CW20+SFS80 blends were 5% and 6.3%, respectively. On this basis, and provided that the surcharge and live loads (e.g. pavement, live loads) are greater than the swell pressure (approximately 50 kPa for CW50+SFS50), vertical

expansion should not occur, and moreover, it is unlikely the swelling potential would influence the performance and stability of the built Port Infrastructure.

2.2 Evaluating CW+FA mixtures for road base/subbase

SFS has a great potential for swelling and its use in ground engineering projects is contingent on the amplitude of live loads to counteract the swelling pressure. Loads at the level of the base/subbase of roads may not be enough to prevent swelling and undesirable deformations. A mixture of CW and fly ash (FA) (CW+FA) is another alternative to natural rock aggregates for base/subbase material in roads, with the FA being added to fill the voids and increase the density of the mixture and improve particle interlocking for increased strength. A comprehensive optimisation study has been carried out on several mixtures of coal wash and fly ash using different amounts of fly ash; this experimental study is summarised in Figure 4 (Wang *et al.*, 2019).

2.2.1 Selecting the optimum FA content

To evaluate the effect that FA has on compaction efficiency, a standard Proctor compaction was carried out on a mixture where the amounts of FA ranged between 0% and 20%. Since the components of this mixture had different specific gravities, the compaction efficiency was represented by the void ratio rather than the dry density. Figure 5 shows that the void ratio decreases as the amount of FA increases up to 10%, after which the void ratio begin to increase again. These preliminary results prove that the optimum amount of FA is around 10%. In practice however, the compaction energy is often higher than the standard Proctor compaction tests, so based on the results of standard Proctor compaction, modified Proctor compaction tests were carried out on smaller amounts of FA (i.e. 7%, 10% and 13%) to mimic field conditions. Figure 5b shows that the minimum void ratio corresponds to 7% FA and 6% water content, however the compaction curve became flatter as the amount of FA increased beyond 7%. This indicates that larger amounts of FA can reduce the compaction efficiency, regardless of water content. The strength and deformation of CW+FA mixtures were further evaluated based on their unconfined compressive strength (UCS), the California Bearing Ratio (CBR), and the collapse potential (CP), to verify that 7% is the optimum amount of FA needed to improve their geotechnical behaviour.

The UCS of CW+FA mixtures compacted at a modified Proctor energy was studied as per AS 5101.4 (Standards Australia 2008). The samples were prepared under different moisture contents in relation to the

OMC determined based on the modified Proctor compaction curve. Moisture contents were selected to cover both the dry side and the wet side of OMC to evaluate the effect of moisture content on the strength of the mixture with varying FA contents (see Table 1). Figure 6a shows that the maximum UCS at OMC (i.e. 6%) corresponds to 7% FA. On the wet side of OMC, the mixture with 7% FA has the highest UCS and the mixture with 13% FA has the highest UCS on the dry side of OMC. However, very dry conditions are not suitable in practice because they induce brittle behaviour that results in tensile cracking. The UCS of the mixture with 7% FA (i.e. 250 kPa) is lower than 1000 kPa, which is the maximum allowed for base/subbase material in roads needed to avoid extreme brittle behaviour. Figure 6b also shows that the minimum axial strain at the maximum UCS corresponds to 7% FA at OMC, and this increases slightly at OMC-2%. On the wet side of OMC the axial strain of all the mixtures increases significantly, which indicates that regardless of the amount of FA, compacted mixtures under very wet conditions cannot improve the deformation characteristics of the mixture to minimize settlements under live load and satisfy the required criteria of 2% maximum axial strain for a base/subbase material (Saberian et al. 2018).

The CBR of CW+FA mixtures with 7%, 10%, and 13% was evaluated under soaked conditions; the results are shown in Figure 6c. The CBR values of CW+FA mixtures with 7%, 10%, and 13% were evaluated under soaked conditions (Figure 6c). The samples were compacted at the OMC under modified Proctor effort and then soaked for 4 days with a 4.5 kg surcharge. Then, the CBR test was performed as per the Australian standards AS 1289.6.1.1 (Standards Australia 2014). The CBR increases when 7% FA is added and then decreases again with larger amounts of FA. Once again this proves that with an optimum amount of FA the strength of the mixture increases due to improved particle interlocking because the FA acts like a void filler. Moreover, the CBR of the mixture with 7% FA is higher than the minimum required for a subbase in roads, whereas the CBR of all the other mixtures is below the required value.

The CP of the CW+FA mixtures was determined using a modified odometer test. In this test an axial load of 200 kPa was applied and then the sample was flooded with water. The CP was determined as the change in the void ratio before and after flooding. Figure 6d shows that the CP of all the mixtures is well below the maximum value (1%) for a base/subbase (Pusadkar and Ramasamy, 2005).

188 *2.2.2 Evaluating the optimum amount of FA*

189 Based on the optimum compaction efficiency and the results of CBR, UCS, and CP tests, the mixture with
190 7% FA was selected as the optimum mixture. In addition to these tests, 2-point bending tests and repeated
191 load tests were carried out on the mixture with 7% FA to further investigate its tensile strength and behaviour
192 under dynamic loading conditions. The tensile strength tests were carried out on the dry side and wet side
193 of the OMC. Figure 7a shows how the maximum tensile strength coincides with the OMC (i.e. 6%), as
194 determined from the modified Proctor compaction tests. When the water content decreases to OMC-1%
195 (80% OMC), the tensile strength also decreases slightly, but there would be a significant drop if the water
196 content decreased to OMC-2% (70% OMC). Similarly, on the wet side of OMC the tensile strength
197 decreased significantly, even with a 1% increase in the water content. It was observed that the tensile strain
198 had decreased slightly on the dry side of OMC, whereas the rate of increase in wet conditions was much
199 higher. Therefore, to sustain a higher tensile strength and avoid tensile cracking and cracks propagating
200 onto the surface of the pavement, the mixture must be placed at OMC or slightly drier than OMC (>80%
201 OMC). Wet conditions must be avoided because they inhibit compaction, induce higher axial and tensile
202 strains, and reduce the tensile strength of the mixture.
203 Repeated load tests (RLT) were carried out as specified by Austroads (2007). These tests consist of 5
204 separate stages of 10,000 cycles per stage; the cyclic deviator stress was increased by 100 kPa at each
205 stage to mimic different loading conditions at the level of the subbase and base layer in roads. Figure 7 (b-
206 c) shows the permanent axial strain and resilient modulus at the end of each stage under four dry-back
207 conditions. When tested at OMC, the strain accumulates at an increasing rate, with an increasing cyclic
208 stress, while the frictional failure commences at the beginning of the fourth stage with a load greater than
209 350 kPa. When the load is below 350 kPa, the axial strain decreases with a decreasing water content up
210 to a dry-back of 80% OMC, and then it increases again with a further dry back to 70% OMC. At a greater
211 load (i.e. > 350 kPa), the minimum axial strain corresponds to 80% OMC, whereas the mixture at 90% OMC
212 exhibits frictional failure, as noted by an increasing rate of strain accumulation. The resilient modulus
213 (Figure 7c) increases as the cyclic deviator stress increases due to the densification experiences at each
214 loading stage; it also increases as the water content decreases. At 80% OMC, the mixture could sustain a
215 resilient modulus ranging from 100 MPa to140 MPa for cyclic loads of 150 kPa and 550 kPa, respectively.

The RLTs show that the mixture is good enough for a subbase with 80% OMC dry-back, but it can only be used as a base if the live loads are less than 350 kPa, i.e., for roads carrying light traffic.

3. Role of Recycled Rubber for Railways

This section mainly focuses on several innovative ways to improve the rail track performance using recycled rubber products, including (i) developing a synthetic energy absorbing layer (SEAL) for railway subballast by adding rubber crumbs (RC) in mining waste (i.e. SFS and CW); (2) using recycled waste tyre cell to reinforce the railway capping layer; and (3) installing under sleeper pads (USP) or under ballast mats (UBM) to reduce the track displacement and ballast degradation. The large-scale process simulation primordial testing apparatus (PSPTA) at the University of Wollongong (UOW) was used to examine the performance of different methods, and the schematic illustration of each method is shown in Figure 8 (b-d).

3.1 SEAL for subballast using SFS+CW+RC mixtures

Indraratna *et al.* (2017a) extended the use of mining waste (SFS and CW) by adding rubber crumbs to mixtures of SFS+CW to develop a synthetic energy absorbing layer (SEAL) for railway subballast. They found that adding rubber $R_b \geq 10\%$ (by weight) to SFS+CW mixtures having SFS:CW=7:3 (the optimal blending ratio, by weight), these waste mixtures of SFS+CW+RC can provide a comparable shear strength to traditional subballast, but without inducing any risk of the SFS swelling and particle breakage of CW (Indraratna *et al.*, 2017a; Qi *et al.*, 2018a; Qi *et al.*, 2019a; Qi *et al.*, 2019b). To better understand the damping property and energy absorption concept of the SFS+CW+RC mixture by adding rubber, a series of small-scale cyclic loading triaxial tests were carried out on these waste mixtures and a large-scale physical model was proposed to verify the enhanced energy absorbing capacity after adding SEAL to a track.

3.1.1 Materials and cyclic testing program

The source materials for SFS and CW are the same as those mentioned in Section 2, whereas the rubber crumbs (RC) shredded from waste tyres provided by Tyre Crumbs Australia came in four sizes (0-2.3 mm, 0.3-3 mm, 4-7 mm, and 8-15 mm). The particle size distribution curves (PSD) of RC, SFS, and CW are shown in Figure 9a. All the waste materials were sieved and separated according to their size ranges. When preparing the samples (50 mm in diameter and 100 mm high) for the cyclic triaxial test, all the mixtures were prepared following the same target PSD (see Figure 9b) by adding the exact weight of each material

(i.e. SFS, CW and RC) according to the different size ranges. The target PSD for the waste mixtures is comparable with traditional subballast materials tested in previous studies, e.g. Trani and Indraratna (2010), Radampola *et al.* (2008) and Kabir *et al.* (2006). The optimal blending ratio of SFS:CW=7:3 was used with varying amounts of RC contents ($R_b = 0, 10, 20, 30,$ and 40%). Each SFS+CW+RC mixture was compacted to around 95% of its maximum dry density after mixed with its optimum water content.

The consolidated drained cyclic triaxial test was in accordance with ASTM-D5311/D5311M (2013). Three confining pressures ($\sigma'_3 = 10, 40,$ and $70\ kPa$) and the cyclic stress ratio ($CSR = q_{cyc,max}/2\sigma'_3$ = 0.8) were used to simulate field conditions. The cyclic loading test was completed up to 50,000 cycles at a frequency of 5 Hz. Details of this test procedure can be found in Indraratna *et al.* (2017a) and Qi *et al.* (2018b).

3.1.2 Damping property and the energy dissipation concept

Damping is the ability of a material to dissipate energy when subjected to a dynamic load. The damping ratio (D) is the key parameter needed to evaluate the damping capacity of waste mixtures, and it can be calculated by using the typical stress-strain hysteresis loop shown in Figure 10a. The total amount of energy dissipated in one loading cycle (E) can be represented by the area of the hysteresis loop (Figure 10a). The typical stress-strain hysteresis loop of SFS+CW+RC mixtures with different RC contents is shown in Figure 10b. It shows that as R_b increases, the hysteresis loop becomes bigger, indicating that more energy has dissipated, and at the same loading cycle, more rubber in the waste mixture causes more vertical strain due to the highly deformable behaviour of rubber materials.

Figure 10c shows D and E of the waste mixture in variation with the loading cycles (N). As expected, the damping ratio and dissipated energy increase as R_b increases. Note that the D and E of the SFS+CW+RC mixture having $R_b = 0\%$ is very stable as N changes, whereas the D and E of waste mixtures with $R_b \geq 10\%$ reduces as N increases and then stabilises at around N=10,000 (Figure 10c). Note also that when an RC of 10% is added to the waste mixture, D increases dramatically, whereas when more RC is included the increase rate in D actually decreases. This is because when after adding a certain amount of RC (>10%) the skeleton of the waste mixture is governed by RC particles, so the mixture tends to behave more like rubber, as suggested by Qi *et al.* (2018b). The influence of σ'_3 on D and E is shown in Figure 10d, where the SFS+CW+RC mixture with $R_b = 10\%$ is used as an example. When σ'_3 increases, the damping ratio decreases but more energy is dissipated, thus indicating that the efficiency of dissipating energy decreases.

It is assumed that under a given track load the total energy input of the track substructure (ballast, subballast and subgrade) is a certain amount. The total energy absorbed or accumulated by a track system will be converted to elastic energy via elastic strain and the dissipated energy (particle breakage, plastic deformation, heat, sound etc.). By taking the SEAL as an example, when R_b increases the dissipated energy increases (Figure 10c) and the elastic energy also increases, as shown by Qi *et al.* (2018b), and thereby the total absorbed energy increases due to the addition of RC. Therefore, by increasing the energy absorbing capacity of the subballast layer using SEAL, the energy transferred to ballast and the subgrade can further decrease, which in turn reduces ballast breakage and associated deformation.

3.1.3 Physical modelling

In order to verify the energy dissipation concept and examine the performance of a track using SEAL as subballast, a physical model was developed and tested using the large-scale process simulation primordial testing apparatus (PSPTA) shown in Figure 8a. The PSPTA testing cell had an area of 600×800 mm and is 600 mm in depth. The physical model consisted of three layers (Figure 8b), i.e. the ballast layer (200 mm thick), the subballast layer (150 mm thick), and the subgrade layer (100 mm thick). A 150mm thick concrete sleeper was placed on top of the test specimen, and around it was filled with the shoulder ballast. The ballast and subgrade materials were from a local quarry near UOW; their PSD is shown in Figure 9a. While preparing the test specimen the PSD of ballast was obtained according to the Australian Standard (AS-2758.7, 2015), and the ballast and subgrade materials were compacted to field conditions. The SEAL mixture (SFS+CW+RC) was used as subballast instead of traditional subballast materials. The target PSD of the SEAL mixture for the large-scale cubical triaxial test is shown in Figure 9b. Five large-scale triaxial tests were carried out, and in each test the amount of RC (0, 10, 20, 30 and 40%) in the SEAL was changed beforehand. A maximum cyclic vertical stress of 230 kPa and a loading frequency of 15 Hz was used to simulate a train with a 25-tonne axle load with a speed of 110 km/h (Indraratna *et al.*, 2014; Navaratnarajah and Indraratna, 2017; Jayasuriya *et al.*, 2019). A lateral confining pressure $\sigma'_3 = 15\ kPa$ was applied in the transverse direction of the track to simulate the pressure provided by the crib and shoulder ballast according to real track conditions (Navaratnarajah *et al.*, 2018). After each test the ballast was sieved to examine the particle breakage. During these tests, only the specimen with 40% RC failed at around 1,500 cycles due to severe vibration and settlement, all the other tests were completed up to 500,000 cycles.

To evaluate the particle degradation of ballast during cyclic loading, the ballast breakage index (BBI) initially proposed by Indraratna *et al.* (2005) was used; the BBI can be calculated based on the PSD before and after the test, the details are shown in Figure 11a. The BBI of the test specimen with different amounts of RC is shown in Figure 11b. As expected, the addition of RC in SEAL significantly reduces the ballast particle breakage more than the one without RC, but when more RC is included in SEAL, there is no significant reduction in BBI and the value for the specimen with 20% RC is even higher; this is probably due to the vibration caused by the rubbery behaviour of the SEAL, as explained earlier. The plastic vertical strain ε_1 of the track specimen is shown in Figure 11c, where ε_1 of the track specimen increases as R_b increases in the SEAL. Note that the failed test specimen with 40% RC had a plastic axial strain of almost 10% even after 1,500 cycles. This indicates that too much RC ($\geq 40\%$) can induce track failure due to excessive settlement and vibration. Compared to the traditional track specimen in the previous study that was tested by Jayasuriya *et al.* (2019) under the same loading conditions, except for the specimen with 0% RC, all the specimens with SEAL having $R_b \geq 10\%$ could reduce the BBI by 40-60% with acceptable vertical deformation. Therefore it is recommended that 10% of RC should be added to the SEAL because it enhance track performance with less ballast breakage and track settlement.

3.2 SEAL for subballast using CW+RC mixtures

3.2.1 Strength and deformation

An alternative method for developing a synthetic energy absorbing layer (SEAL) using CW and RC only, is also possible for the subballast/capping layer, however, since CW is weaker than SFS, removing SFS from the blend would affect the strength and deformation of the mixture. Compaction tests and monotonic triaxial tests were carried out on four CW+RC mixtures with 0%, 5%, 10% and 15% rubber to evaluate its effect on the geotechnical behaviour of a CW+RC mixture (Indraratna *et al.*, 2019b). Indraratna *et al.* (2019b) proved that the mixture can be compacted to an acceptable void ratio by increasing the compaction energy without inducing excessive breakage, so triaxial tests were then carried out under three confining pressures to mimic different field conditions (i.e. 25, 50 and 75 kPa). All the mixtures were compacted to the same void ratio to examine how the amount of rubber would affect the stress-strain response.

Figure 12a shows the stress-strain relationship of CW+RC mixtures at a confining pressure of 50 kPa. It is noted that the inclusion of RC improves the ductility of the material. Ductility prevents tensile cracking and

328 sudden and brittle failure when a mixture is subjected to a long lifecycle and when it reaches a state of
329 fatigue. For the CW+SFS+RC mixture tested by Indraratna *et al.* (2017a), the peak deviator stress
330 decreases as the amount of rubber increaseds, however Figure 12b shows that the peak deviator stress of
331 all the mixtures is greater than the maximum axial stress expected at the level of the subballast/capping
332 layer.
333 The inclusion of rubber particles induce higher deformation under the same stress because the rubber
334 compresses and become deformed. The axial strain at the peak deviator stress plotted in Figure 12c shows
335 that the axial strain increases as the amount of rubber increases. The maximum allowable settlement of
336 the subballast/capping layer is 2%. In Figure 12d, the deviator stress that corresponds to an axial strain of
337 2% is plotted. For an amount of RC ≤ 10% and the confining pressure usually observed in practice (i.e. 40-
338 50 kPa), the mixture can sustain a stress that is higher than the expected stress at the level of the
339 subballast/capping layer with an axial deformation of 2%. This indicates that the inclusion of rubber does
340 not induce excessive settlement if the amount of RC is less than 10%.
341 *3.2.2 Energy absorption*
342 The main reason for using recycled rubber in infrastructure sublayers is to minimise particle degradation
343 and increase the energy absorbing potential of the material. Figure 13 shows the Breakage Index (BI) and
344 the energy absorbing potential of CW+RC mixtures. The BI was determined after compaction based on the
345 method proposed by Indraratna *et al.* (2005) and the energy absorbing capacity was evaluated based on
346 the maximum work absorbed by the mixture up to the point of failure (Indraratna *et al.*, 2019b). Figure 13a
347 shows that the BI decreases by approximately 50% when 10% of RC is added, after which there is no
348 significant decrease in breakage. This indicates that an amount of rubber of more than 10% is unnecessary
349 because it only induces higher axial settlement without any further reduction in degradation. The energy
350 absorbing potential shown in Figure 13b indicates that the capacity of the mixture to absorb energy
351 increases as the amount of rubber increases. This increase is more evident at higher confining pressures
352 due to an increase in the compressibility of rubber. An energy absorbing layer is of great benefit in corridors
353 that generate vibration, such as railways. Previous studies showed there was much less vibration when a
354 layer of rubber was introduced into the track (Cho *et al.*, 2007). Similarly, a SEAL matrix helps to attenuate

noise and vibration so there is less disturbance in the surrounding environment at sites where a railway track is very close to residential or commercial areas.

3.3 Waste tyre cell-reinforced capping layer for heavy haul loading

3.3.1 Materials and test loading conditions

An innovative method for confining the capping layer (subballast) using recycled tyre cells has been proposed by (Indraratna *et al.*, 2017c, Sun et al., 2019). The aim is to reduce particle movement and ballast degradation, and increase the stability and resiliency of track infrastructure. Large-scale cyclic cubical triaxial tests using PSPTA were carried out to evaluate a capping layer confined with tyre cells; this large-scale triaxial sample contained a ballast layer, a capping layer, and a subgrade layer (Figure 8c). The ballast and capping layers are crushed basalt (latite) with particle sizes ranging from 2.36-53 mm and 0.075-19 mm, respectively. The bottom layer is a 50-mm thick subgrade layer. The cyclic loading test proceeded under two different conditions, a traditional track specimen confined with and without a recycled tyre cell. One sidewall of the recycled tyre was removed and the tyre was filled with traditional capping materials (i.e. crushed basalt). A woven geotextile was installed at the interface of the capping layer and the structural fill to serve as a separator.

The cyclic loading tests carried out at 15 Hz, and a maximum axial stress $\sigma'_{1cyc,max} = 385\ kPa$ and a minimum axial stress $\sigma'_{1cyc,min} = 15\ kPa$ were applied to simulate a heavy haul train with an axle load of 40 tonnes (Jeffs and Tew, 1991). Each cyclic loading test consisted of 500,000 cycles, after which the ballast was sieved to determine the extent of degradation.

3.3.2 Test results

Figure 14a shows the results of the cubical triaxial test in terms of the lateral and vertical deformation of the specimens where lateral displacement without a tyre cell increases rapidly at the beginning of the test and then stabilises around N=100,000 cycles. As expected, there is a dramatic reduction in the lateral displacement of the specimen with a tyre cell because the particles are confined and therefore tend to contract more. The vertical settlement develops rapidly during the first thousands of loading cycles and then gradually stabilises after 100,000 cycles. It is noteworthy that the specimen reinforced with a tyre cell experiences a greater reduction in the vertical displacement (around 10-12 mm) than the specimen without

a tyre cell. Overall, these test results indicate that the additional confinement provided by a tyre cell can reduce track settlement and lateral displacement.

The damping ratio (D) and dissipated energy (E) of the test specimen confined with and without a tyre cell are shown in Figure 14b. The tests show that when a track is confined by a tyre cell the damping property is enhanced and the dissipated energy increases. When the test begins, the D and E decrease as the number of loading cycles increase due to the high dissipation of energy caused by plastic sliding and particle breakage, but when there are more than 10,000 loading cycles the D and E are almost constant because the granular mass becomes dense and stable.

Ballast could experience significant degradation during long-term service due to repeated loading (Indraratna *et al*., 2011), but since tyre cells have a higher damping property they can reduce ballast degradation. The PSD of ballast before and after the test, and the BBI values of specimens with and without a tyre cell are shown in Figure 15, here the PSD curves indicate that the biggest change in the size of ballast took place in the 37.5 mm sieve. The BBI of the specimen confined with a tyre cell is almost 70% less than the specimen without a tyre cell. This result suggests that a ballast layer could become more durable if the capping layer is reinforced by energy absorbing tyre cells, a result that would reduce the amount of aggregates taken from a quarry.

3.4 Using rubber mats/pats to improve the performance of track with stiff subgrade

3.4.1 Under sleeper pads and under ballast mats testing program

A series of tests to investigate the effect of under sleeper pads (USP) and under ballast mats (UBM) for rail track built on the stiff subgrade such as tunnels and bridges were carried out using PSPTA. The test specimen contained two layers: (i) a 300 mm thick ballast layer, and (ii) a 150 mm thick concrete base to simulate a rail track on a stiff subgrade. The position of the USP and UBM is also shown in Figure 8d. The ballast material tested was the same mentioned in the previous section. The USP and UBM were manufactured from recycled waste tyres. The rubber mats/pats were made by encapsulating waste rubber granulates in a polyurethane elastomer compound. The USP and UBM were 200×800 mm by 10 mm thick, and 600×800 mm by 10 mm thick, respectively. Cubical triaxial tests were conducted with USP, with UBM, and without any rubber inclusions. The maximum vertical stress at the sleeper-ballast interface was 230 kPa to simulate a train with a 25-tonne axle load. The influence of frequency was captured by varying the

loading frequency (i.e. 15, 20, and 25 Hz). Each test was carried out up to 500,000 cycles, after which the ballast was sieved to check the particle degradation.

3.4.2 Deformation, damping property and ballast degradation

The settlement and lateral displacement of the test specimen without rubber inclusions, and with USP or UBM under different loading frequencies are shown in Figure 16 (a-b). Since the concrete base is regarded as rigid, the deformation recorded here only refers to the ballast layer. The test results indicate that the ballast quickly deforms vertically and laterally up to around 10,000 cycles and remains relatively constant after 100,000 cycles. Note that when increasing the loading frequency, the test specimen becomes more deformed. It is evident that the addition of USP and UBM helps to reduce the vertical and lateral deformation of ballast by a considerable amount. Specifically, under a loading frequency of 15-25 Hz the inclusion of USP reduces the vertical deformation by 16-47% and the lateral displacement by 21.5-55%, as opposes to a 20-34% reduction in vertical deformation and 39-44% in lateral displacement using UBM.

To better understand how the USP and UBM influence the energy absorbing properties of a rail track, the D and E of the test specimen were examined (Figure 16 c-d). The results indicate that D and E are initially high at the beginning of the test, but decrease as N increases, and then stabilize at around N=100,000. This can be attributed to the particle sliding and breakage which consumed a lot of energy at the initial stage. Note that the inclusion of rubber mats/pats increases the damping capacity of the track and causes a higher dissipation of strain energy. Overall, the track specimen with USP has a higher damping property and energy dissipation than the track with UBM; this indicates that having a rubber mat under the sleeper is a better way of enhancing the energy absorbed by the rail track. This can be further reflected by investigating ballast degradation. Figure 17 shows the ballast breakage index (BBI) of the test specimen under various loading frequencies; as expected, increasing the loading frequency increases the BBI and the addition of rubber mats/pats significantly reduces ballast degradation. It is evident that the addition of the USP reduces ballast breakage by more than 50% while using UBM reduces ballast degradation by almost 19-23%.

Overall, the use of rubber mats/pats in a track enhances its performance by reducing the deformation, increasing the damping property, and reducing particle breakage. However, these enhanced performances depend mainly on the physical properties of the rubber mat/pat (e.g. its thickness, stiffness, and density),

its position (i.e. USP or UBM), and the stiffness of the subgrade (e.g. soft or stiff conditions). Hunt and Wood (2005) indicated that using an elastic element to reduce the stiffness or increasing the thickness of the elastic layer can induce excessive deformation and fatigue damage of track components. In practice, UBM is more effective when the subgrade is stiff, i.e. tunnel or bridge conditions (Navaratnarajah and Indraratna, 2017), while the stiffer USP provides a better overall performance (Jayasuriya *et al.*, 2019). The results of this study indicate that by including USP or UBM, the test specimen appears to have a comparable deformation behaviour whereas the USP will increase the damping property more and thus reduce ballast degradation more.

4. Conclusions

This paper has presented some innovative applications for using waste materials (i.e. steel furnace slag, coal wash, fly ash, rubber crumbs, recycled tyre cell and rubber mats/pats) in transportation infrastructures such as using the CW-based granular matrix (SFS+CW or CW+FA) for port reclamation and road subbase, rubber crumbs blended with mining waste (i.e. SFS and CW) to replace traditional subballast, under sleeper pads (USP) or under ballast mats (UBM) to minimise ballast deformation and degradation, and waste tyre cells to reinforce the subballast layer. The following important findings can be drawn from this paper:

- While compacted coal wash exhibited sufficient shear strength for the Port infrastructure, there was still excessive breakage during shearing when the levels of confinement exceeded 127kPa. To address this shortcoming, blends of compacted CW and SFS were considered. The blends with 30-45% of SFS content demonstrate sufficient performance to meet the stringent in-service requirements for Port infrastructure while minimising the effect of breakage and swelling.
- A mixture of CW and FA is a possible alternative for road infrastructure sublayers. An optimum of 7% of FA and 6% of OMC were selected based on compaction, CBR, UCS and CP tests. The tensile strength tests show that this mixture must be at the OMC or slightly drier than OMC to prevent tension cracking and sustain the highest tensile strength. The mixture was further tested under cyclic loading to mimic field conditions, with the tests showing that the mixture is adequate for a subbase layer if a dry-back condition of 80% OMC is applied. The mixture can only be used as base material if the loads are not expected to exceed 350 kPa.
- Two methods were provided for a synthetic energy absorbing layer (SEAL), i.e. a SFS+CW+RC mixture

and a CW+RC mixture. The cyclic triaxial tests showed that by increasing the amount of RC in the waste mixture, the damping property and the dissipated energy increased, indicating that by using the SFS+CW+RC matrix it would help to reduce track degradation. This was verified by a large-scale physical model which proved that adding 10% of RC in the waste mixture enabled the test specimen to have less ballast degradation and track deformation than the traditional track specimen. As with the CW+SFS+RC mixture, monotonic triaxial tests showed that adding 10% of rubber to a CW+RC mixture compacted with higher energy yielded an acceptable axial deformation for the subballast/capping layer and reduced particle degradation by approximately 50% more than those without RC. Most importantly, with the enhanced energy absorption potential of the CW+RC mixture, it can provide a promising inclusion for damping and reducing the vibration generated by passing trains.

- Large-scale cubical triaxial tests were also carried out to investigate the performance of the track specimen reinforced with tyre cells under a heavy haul loading condition. The tests indicated that tyre cells infilled with traditional capping layer materials can provide considerable lateral confinement and reduce the vertical settlement of a track by approximately 10-12 mm compared to the sample without tyre cells. Moreover, tyre cells can significantly reduce ballast degradation by more than half.
- The large-scale cubical triaxial tests of a track with stiff subgrade and stabilised with USP or UBM had enhanced track performance with less vertical and lateral deformation, higher damping properties, and less ballast degradation. By increasing the loading frequency, the deformation and ballast degradation increase. Overall, adding USP or UBM provided a comparable deformation (vertical and lateral) of the track specimen, whereas USP showed a more promising result for its damping capacity and ballast degradation.

488 **List of Acronyms:**

BBI= Ballast breakage index;
BI= Breakage index;
BOF= Basic Oxygen Furnaces;
BOS= Basic oxygen slag;
CBR= California Bearing Ratio;
CP= Collapse potential;
CSR= Cyclic stress ratio;
CW= Coal wash;
DCPT= Dynamic Cone Penetration Test;
EAF= Electric Arc Furnaces;
FA= Fly ash;
OMC= Optimum moisture content;
PLT= Plate Load Test;
PSD= Particle size distribution;
PSPTA= Process simulation primordial testing apparatus;
RC= Rubber crumbs;
RLT= Repeated load tests;
ROM= Run-of-mine;
SEAL= Synthetic energy absorbing layer;
SFS= Steel furnace slag;
UBM= Under ballast mats;
UCS= Unconfined compressive strength;
UOW= University of Wollongong;
USP= Under sleeper pads.

489

Acknowledgements

The authors would like to acknowledge the financial assistance provided by the Australian Research Council (ARC) Discovery Project (ARC-DP180101916), ARC Linkage Project (LP160100280) and ARC Industry Transformation Training Centre for Advanced Rail Track Technologies (ARC-ITTC-Rail). The assistance provided by industry (Port Kembla Port Corporation (PKPC), Menard Bachy, Coffey Geotechnics, RMS, Douglas Partners, ASMS, South 32, Ecoflex Australia and Tyre Crumbs Australia) in relation to the procurement of material used in this study is gratefully acknowledged. The laboratory assistance provided by Mr Richard Berndt, Mr Cameron Neilson, Mr Jordan Wallace, Mr Quang Minh Vu and Mr Salvatore Wedde is appreciated. The content of this paper has been the result the research on the reuse of waste materials in transport infrastructure carried out at the University of Wollongong for a number of years which are partially reproduced from published work with kind permission from ASCE Journal of Geotechnical and Geoenvironmental Engineering, ICE Ground Improvement, and Transportation Geotechnics. The authors would like to acknowledge the contributions from past PhD students and Research Associates, namely Dr Chazath Kaliboullah, Dr Ali Tasalloti, Dr Gabrielle Chiaro, Dr Qideng Sun, Dr Chamindi Jayasuriya and Dr Jayan Vinod, as well as industry partners namely Geoff McIntosh (Douglas Partners), Phillip Vincent (Menard Group), Tonilee Andrews (PKPC), Jim Grant (Ecoflex), Peter Meers and Robyn Lyster (Roads and Maritimes Services).

References

Ahmaruzzaman, M. (2010). A review on the utilization of fly ash. *Progress in energy and combustion science* **36**(3): 327-363.

Arulrajah, A., Maghool, F., Mohammadinia, A., Mirzababaei, M. and Horpibulsuk, S. (2020a). Wheel tracker testing of recycled concrete and tyre aggregates in Australia. *Geotechnical Research*: 1-9.

Arulrajah, A., Naeini, M., Mohammadinia, A., Horpibulsuk, S. and Leong, M. (2020b). Recovered plastic and demolition waste blends as railway capping materials. *Transportation Geotechnics*: 100320.

AS-2758.7 (2015). Aggregates and rock for engineering purposes, Part 7: Railway ballast. Sydney, New South Wales, Australia, Standard Australia.

ASTM-D5311/D5311M (2013). Standard test method for load controlled cyclic triaxial strength of soil, ASTM International West Conshohocken, PA.

ASTM D6951/D6951M (2009). Standard test method for use of the dynamic cone penetrometer in shallow pavement application, West Conshohocken, PA, USA.

Austroads (2007). Determination of permanent deformation and resilient modulus characteristics of unbound granular materials under drained conditions. AGPT-T053-07. Austroads, NSW, Australia.

Brulliard, C., Cain, R., Do, D., Dornom, T., Evans, K., Lim, B., Olesson, E., Young, S. and Balance, N. (2012). The Australian recycling sector. *Net Balance; Department of Sustainability, Environment, Water, Population and Communities*.

Chiaro, G., Indraratna, B., Tasalloti, S. and Rujikiatkamjorn, C. (2015). Optimisation of coal wash-slag blend as a structural fill. *Proceedings of the Institution of Civil Engineers: Ground Improvement* **168**(GI1): 33-44.

Cho, S. D., Kim, J. M., Kim, J. H. and Lee, K. W. (2007). Utilization of waste tires to reduce railroad vibration. Materials science forum, Trans Tech Publ.

Costa, P. A., Calçada, R. and Cardoso, A. S. (2012). Ballast mats for the reduction of railway traffic vibrations. Numerical study. *Soil Dynamics and Earthquake Engineering* **42**: 137-150.

Davies, P., Philip, R. E. D. and James, D. M. (2011). Geotechnical design for the Port Botany expansion project, Sydney. *Proceedings of the Institution of Civil Engineers. Geotechnical engineering* **164**(9): 149 –167.

Downs, L.A., Humphrey, D.N., Katz, L.E. and Rock, C.A. (1996). Water quality effects of using tire chips below the groundwater table, Technical Services Division, Technical Paper. A Study For The Maine Department Of Transportation.

Edil, T.B. and Bosscher, P.J. (1992). *Development of Engineering Criteriafor Shredded or Whole Tires in Highway Applications*, Report No.WI 14-92, Department of Civil and Environmental Engineering, University of Wisconsin, Madison, WI.

Fityus, S., Hancock, G., and Wells, T. (2008). Geotechnical characteristics of coalmine spoil. *Aust. Geomech.*, 43(3): 13–22.

Heitor, A., Indraratna, B., Kaliboullah, C. I., Rujikiatkamjorn, C. and McIntosh, G. W. (2016). Drained and undrained shear behavior of compacted coal wash. *Journal of Geotechnical and Geoenvironmental Engineering* **142**(5): 04016006.

Heitor, A., Indraratna, B., Rujikiatkamjorn, C., Chiaro, G. and Tasalloti, S. A. (2014). Evaluation of the coal wash and steel furnace slag blends as effective reclamation fill for port expansion. In A. Bouazza, S. T. S. Yuen & B. Brown (Eds.), 7th International Congress on Environmental Geotechnics (pp. 972-979). Melbourne, Australia: Engineers Australia.

Humphrey, D.N., Katz, L.E. and Blumenthal, M. (1997). Water quality effects of tire chip fills placed above the ground water table, In: Wasemiller Mark A, Hoddinott Keirh B, editors. Testing soil fixed with waste or recycled materials, ASTMSTP1275. American Society for Testing and Materials.

Hunt, G. and Wood, J. (2005). Review of the effect of track stiffness on track performance. *RSSB, Research Project* **372**.

Indraratna, B. (1994). Geotechnical characterization of blended coal tailings for construction and rehabilitation work. *Quarterly Journal of Engineering Geology and Hydrogeology* **27**(4): 353-361.

557 Indraratna, B., Biabani, M. M. and Nimbalkar, S. (2014). Behavior of geocell-reinforced subballast subjected
558 to cyclic loading in plane-strain condition. *Journal of Geotechnical and Geoenvironmental Engineering*
559 **141**(1): 04014081.
560 Indraratna, B., Ferreira, F. B., Qi, Y. and Ngo, T. N. (2018). Application of geoinclusions for sustainable rail
561 infrastructure under increased axle loads and higher speeds. *Innovative Infrastructure Solutions* **3**(1):
562 69.
563 Indraratna, B., Gasson, I. and Chowdhury, R. (1994). Utilization of compacted coal tailings as a structural
564 fill. *Canadian Geotechnical Journal* **31**(5): 614-623.
565 Indraratna, B., Lackenby, J. and Christie, D. (2005). Effect of confining pressure on the degradation of
566 ballast under cyclic loading. *Géotechnique* **55**(4): 325-328.
567 Indraratna, B., Ngo, N. T. and Rujikiatkamjorn, C. (2011). Behavior of geogrid-reinforced ballast under
568 various levels of fouling. *Geotextiles and geomembranes* **29**(3): 313-322.
569 Indraratna, B., Qi, Y. and Heitor, A. (2017a). Evaluating the properties of mixtures of steel furnace slag,
570 coal wash, and rubber crumbs used as subballast. *Journal of Materials in Civil Engineering* **30**(1):
571 04017251.
572 Indraratna, B., Qi, Y., Ngo, T. N., Rujikiatkamjorn, C., Neville, T., Ferreira, F. B. and Shahkolahi, A. (2019a).
573 Use of Geogrids and Recycled Rubber in Railroad Infrastructure for Enhanced Performance.
574 *Geosciences* **9**(1): 30.
575 Indraratna, B., Rujikiatkamjorn, C., Tawk, M. and Heitor, A. (2019b). Compaction, degradation and
576 deformation characteristics of an energy absorbing matrix. *Transportation Geotechnics* **19**: 74-83.
577 Indraratna, B., Sun, Q. and Grant, J. (2017b). Behaviour of subballast reinforced with used tyre and
578 potential application in rail tracks. *Transportation Geotechnics* **12**: 26-36.
579 Indraratna, B., Sun, Q., Heitor, A. and Grant, J. (2017c). Performance of rubber tire-confined capping layer
580 under cyclic loading for railroad conditions. *Journal of Materials in Civil Engineering* **30**(3): 06017021.
581 Jayasuriya, C., Indraratna, B. and Ngo, T. N. (2019). Experimental Study to Examine the Role of Under
582 Sleeper Pads for Improved Performance of Ballast under Cyclic Loading. *Transportation Geotechnics*
583 **19**: 61-73.
584 Jeffs, T. and Tew, G. (1991). A Review of Track Design Procedures-Sleepers and Ballast, Vol. 2, Railways
585 of Australia, Australian Government Publishing Service, Melbourne.
586 Kabir, E., Haque, A. and Bouazza, A. (2006). Effect of cyclic loading on filtration behaviour of subballast
587 material. *Advances in Unsaturated Soil, Seepage, and Environmental Geotechnics***:** 180-186.
588 Kaliboullah, C. I., Indraratna, B., Rujikiatkamjorn, C., and Heitor, A. (2015). Evaluation of coalwash as a
589 potential structural fill material for port reclamation. Proc., 12th Australia New Zealand Conf. on
590 Geomechanics (ANZ 2015), Wellington, New Zealand: 199–206.
591 Malasavage, N. E., Jagupilla, S., Grubb, D. G., Wazne, M. and Coon, W. P. (2012). Geotechnical
592 performance of dredged material—steel slag fines blends: laboratory and field evaluation. *Journal of*
593 *Geotechnical and Geoenvironmental Engineering* **138**(8): 981-991.

Mudd, G. M. (2010). The environmental sustainability of mining in Australia: key mega-trends and looming constraints. *Resources Policy* **35**(2): 98-115.

Naeini, M., Mohammadinia, A., Arulrajah, A., Horpibulsuk, S. and Leong, M. (2020). Stiffness and strength characteristics of demolition waste, glass and plastics in railway capping layers. *Soils and Foundations*: https://doi.org/10.1016/j.sandf.2019.12.009.

Navaratnarajah, S. K. and Indraratna, B. (2017). Use of rubber mats to improve the deformation and degradation behavior of rail ballast under cyclic loading. *Journal of geotechnical and geoenvironmental engineering* **143**(6): 04017015.

Navaratnarajah, S. K., Indraratna, B. and Ngo, N. T. (2018). Influence of under sleeper pads on ballast behavior under cyclic loading: experimental and numerical studies. *Journal of Geotechnical and Geoenvironmental Engineering* **144**(9): 04018068.

Nimbalkar, S. and Indraratna, B. (2016). Improved performance of ballasted rail track using geosynthetics and rubber shockmat. *Journal of Geotechnical and Geoenvironmental Engineering* **142**(8): 04016031.

NSW Environment Protection Authority (EPA) (2014a). Resource Recovery Exemption, the Protection of the Environment Operations (Waste) Regulation 2014 - The coal washery rejects exemption (*http://www.epa.nsw.gov.au/resources/waste/rre14-coal-wash-rejects.pdf).*

NSW Environment Protection Authority (EPA) (2014b). Resource Recovery Exemption the Protection of the Environment Operations (Waste) Regulation 2014 - The steel furnace slag exemption (*http://www.epa.nsw.gov.au/resources/waste/rre14-steel-furnace-slag.pdf).*

Pusadkar, S. S. and Ramasamy, G. (2005). Collapse behavior of compacted coal ash fills. *Geotechnical Testing Journal* **28**(3): 297-304.

Qi, Y., Indraratna, B. and Coop, M. R. (2019a). Predicted Behavior of Saturated Granular Waste Blended with Rubber Crumbs. *International Journal of Geomechanics* **19**(8): 04019079.

Qi, Y., Indraratna, B., Heitor, A. and Vinod, J. (2019b). The influence of rubber crumbs on the energy absorbing property of waste mixtures. Geotechnics for Transportation Infrastructure. Sundaram R., S. J., Havanagi V. Singapore, Springer. **29:** 271-281.

Qi, Y., Indraratna, B., Heitor, A. and Vinod, J. S. (2018a). Closure to "Effect of Rubber Crumbs on the Cyclic Behavior of Steel Furnace Slag and Coal Wash Mixtures" by Yujie Qi, Buddhima Indraratna, Ana Heitor, and Jayan S. Vinod. *Journal of Geotechnical and Geoenvironmental Engineering* **145**(1): 07018035.

Qi, Y., Indraratna, B., Heitor, A. and Vinod, J. S. (2018b). Effect of rubber crumbs on the cyclic behavior of steel furnace slag and coal wash mixtures. *Journal of Geotechnical and Geoenvironmental Engineering* **144**(2): 04017107.

Qi, Y., Indraratna, B. and Vinod, J. S. (2018c). Dynamic Properties of Mixtures of Waste Materials. In: Qiu T., Tiwari B., Zhang Z. (eds) Proceedings of GeoShanghai 2018 International Conference: Advances in Soil Dynamics and Foundation Engineering. GSIC 2018. pp. 308-317. Springer, Singapore.

Radampola, S. S., Gurung, N., McSweeney, T. and Dhanasekar, M. (2008). Evaluation of the properties of railway capping layer soil. *Computers and Geotechnics* **35**(5): 719-728.

631 Rujikiatkamjorn, C., Indraratna, B. and Chiaro, G. (2013). Compaction of coal wash to optimise its utilisation
632 as water-front reclamation fill. *Geomechanics and Geoengineering* **8**(1): 36-45.
633 Saberian, M., Li, J., Nguyen, B., and Wang, G. (2018). Permanent deformation behaviour of pavement base
634 and subbase containing recycle concrete aggregate, coarse and fine crumb rubber. *Construction and*
635 *Building Materials*: **178**, 51-58.
636 Schneider, P., Bolmsvik, R. and Nielsen, J. C. (2011). In situ performance of a ballasted railway track with
637 under sleeper pads. *Proceedings of the Institution of Mechanical Engineers, Part F: Journal of Rail and*
638 *Rapid Transit* **225**(3): 299-309.
639 Sol-Sánchez, M., Moreno-Navarro, F., Pérez, R. and Rubio-Gámez, M. (2019). Defining the process of
640 including sustainable rubber particles under sleepers to improve track behaviour and performance.
641 *Journal of Cleaner Production* **227**: 178-188.
642 Sol-Sánchez, M., Moreno-Navarro, F. and Rubio-Gámez, M. C. (2015). The use of elastic elements in
643 railway tracks: A state of the art review. *Construction and building materials* **75**: 293-305.
644 Standards Australia (2008). Methods for Preparation and Testing of Stabilized Materials—Unconfined
645 Compressive Strength of Compacted Materials. Standards Australia Limited Sydney, Australia.
646 Standards Australia (2014). Methods of testing soils for engineering purposes - Soil strength and
647 consolidation tests - Determination of the California Bearing Ratio of a soil - Standard laboratory method
648 for a remoulded specimen. Standards Australia Limited, Sydney, Australia.
649 Suddeepong, A., Sari, N., Horpibulsuk, S., Chinkulkijniwat, A. and Arulrajah, A. (2020). Interface shear
650 behaviours between recycled concrete aggregate and geogrids for pavement applications. *International*
651 *Journal of Pavement Engineering* **21**(2): 228-235.
652 Sun, Q., Indraratna, B., Heitor, A. (2019) Behaviour of a capping layer reinforced with recycled tyres,
653 *Ground improvement*: 1-32. https://doi.org/10.1680/jgrim.18.00030.
654 Tasalloti, S.M.A., Indraratna, B., Chiaro, G. and Heitor, A. (2015a). Field investigation on compaction and
655 strength performance of two coal wash-BOS slag mixtures. International Foundations Congress and
656 Equipment Expo 2015, IFCEE 2015; San Antonio; United States, Geotechnical Special Publication
657 Volume 256, 2015: 2359-2368.
658 Tasalloti, S. M., Indraratna, B., Rujikiatkamjorn, C., Heitor, A. and Chiaro, G. (2015b). A laboratory study
659 on the shear behavior of mixtures of coal wash and steel furnace slag as potential structural fill.
660 *Geotechnical Testing Journal* **38**(4): 361-372.
661 Trani, L. D. O. and Indraratna, B. (2010). Assessment of subballast filtration under cyclic loading. *Journal*
662 *of Geotechnical and Geoenvironmental Engineering* **136**(11): 1519-1528.
663 Wang, D., Tawk, M., Indraratna, B., Heitor, A. and Rujikiatkamjorn, C. (2019). A mixture of coal wash and
664 fly ash as a pavement substructure material. *Transportation Geotechnics* **21**: 100265.
665 Wang, G. (2010). Determination of the expansion force of coarse steel slag aggregate. *Construction and*
666 *Building Materials* **24**(10): 1961-1966.

667 Xue, Y., Wu, S., Hou, H. and Zha, J. (2006). Experimental investigation of basic oxygen furnace slag used
668 as aggregate in asphalt mixture. *Journal of Hazardous Materials* **138**(2): 261-268.
669 Yildirim, I. Z. and Prezzi, M. (2015). Geotechnical properties of fresh and aged basic oxygen furnace steel
670 slag. *Journal of Materials in Civil Engineering* **27**(12): 04015046.
671

672

673 Table 1 Sample properties for the UCS tests

Test	**UCS**	
FA content (%)	Moisture content (%)	Dry density (g/cm^3)
0	4.98	1.76
	6.50	1.77
	8.34	1.76
	11.26	1.71
7	4.46	1.79
	6.06	1.81
	8.64	1.77
	10.17	1.73
10	4.63	1.77
	7.09	1.77
	8.97	1.78
	10.67	1.74
13	5.04	1.75
	7.45	1.75
	9.23	1.75

674

675 **Figure captions**

676 Figure 1. Particle size distribution and typical aspect of steel furnace slag (SFS) and coal wash (CW)
677 granular waste by-products (modified after Tasalloti *et al*, 2015a).
678 Figure 2. Criteria for defining the optimal CW-SFS blend (modified after Chiaro *et al*., 2015).
679 Figure 3. Photos of the field trial (a) spreading mixed materials, (b) compaction; (c-d) Variation of the
680 equivalent in-situ CBR with depth and (e-f) variation of pressure against settlement for CW50-BOS50 and
681 CW20-BOS80 (modified after Tasalloti *et al*., 2015b).
682 Figure 4. Experimental study for the optimization of a CW+FA mixture (modified after Wang *et al.* 2019).
683 Figure 5. Compaction characteristics of CW+FA at (a) standard proctor and (b) modified Proctor.
684 Figure 6. (a) Unconfined compressive strength, (b) maximum axial strain, (c) Soaked CBR and (d) collapse
685 potential of CW+FA mixtures (modified after Wang *et al.* 2019).
686 Figure 7. (a) Tensile strength, (b) Permanent deformation and (c) resilient modulus of CW+FA mixture with
687 7% FA at different dry-back conditions.
688 Figure 8. (a) Process simulation primordial testing apparatus (PSPTA) at the University of Wollongong, and
689 schematic illustration of (b) the physical model with SEAL, (c) the prismoidal triaxial box reinforced with a
690 recycled tyre cell, and (d) the prismoidal triaxial box with rubber mats.
691 Figure 9. (a) PSD for ballast, subgrade, and waste materials; (b) PSD for traditional subballast and target
692 SEAL PSD for small and cubical triaxial tests.
693 Figure 10. (a) Definition of damping ratio and dissipated energy; (b) hysteresis loops of the waste mixture
694 having different RC contents, and damping ratio and dissipated energy of (c) SFS+CW+RC mixtures.
695 having different RC contents under $\sigma'_3 = 70\ kPa$, and (d) SFS+CW+RC mixtures having 10% RC under
696 different σ'_3.
697 Figure 11. (a) Definition of BBI; cubical triaxial test result of (b) BBI and (c) plastic vertical strain.
698 Figure 12. (a) Stress-strain curve at a confining pressure of 50 kPa and (b) peak deviator stress at
699 different confining pressures, (c) axial strain at q_{peak} and (d) q_{peak} at 2% axial strain of CW+RC mixtures.
700 Figure 13. (a) Breakage Index (BI) and (b) energy absorption potential of CW+RC mixtures.
701 Figure 14. Cyclic cubical triaxial test results of the test specimen with and without tyre cell: (a) lateral
702 displacement and settlement, and (b) damping ratio and dissipated energy (modified after Indraratna *et*
703 *al.,* 2017c).
704 Figure 15. (a) The gradation of ballast before and after test; (b) BBI (data sourced from Indraratna *et al.,*
705 2017c).
706 Figure 16. Cubical triaxial test results of the test specimen with USP or UBM or without rubber mats: (a)
707 settlement and (b) lateral displacement, (c) damping ratio, and (d) dissipated energy (data sourced from
708 Jayasuriya *et al.,* 2019 and Navaratnarajah and Indraratna, 2017).
709 Figure 17. BBI of the test specimen with USP or UBM or without rubber mats.
710

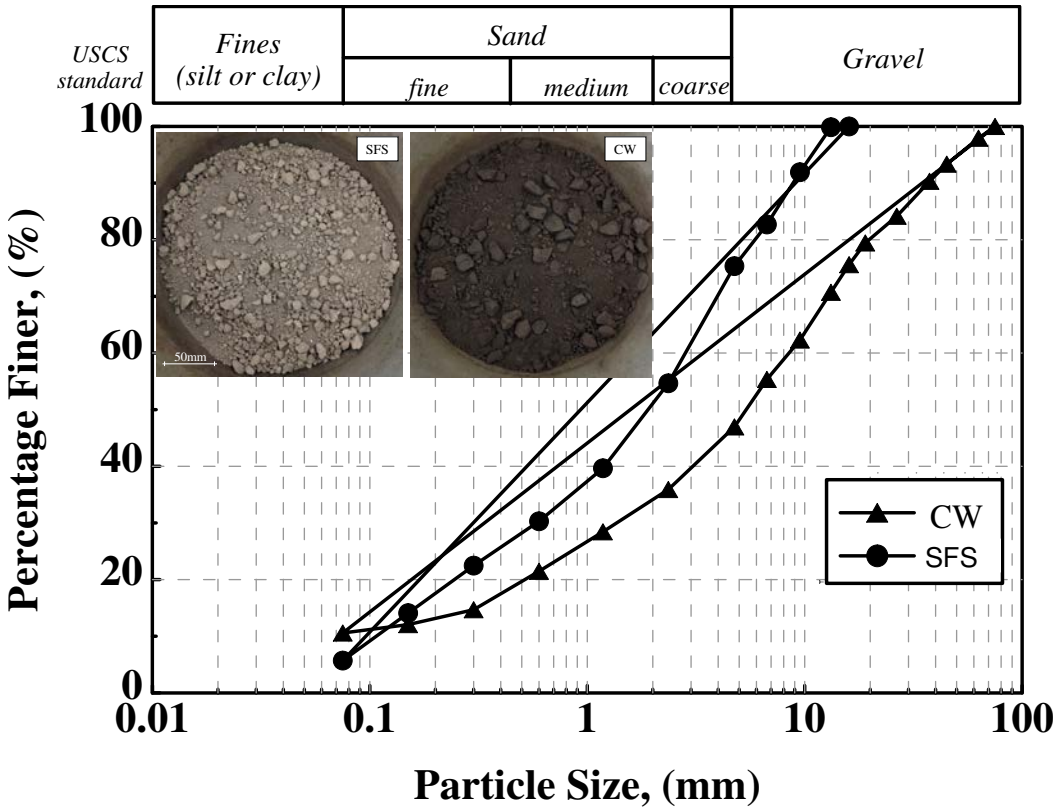

711

712 Figure 1. (a) Particle size distribution and typical aspect of steel furnace slag (SFS) and coal wash (CW)
713 granular waste by-products (modified after Tasalloti *et al*, 2015a).
714

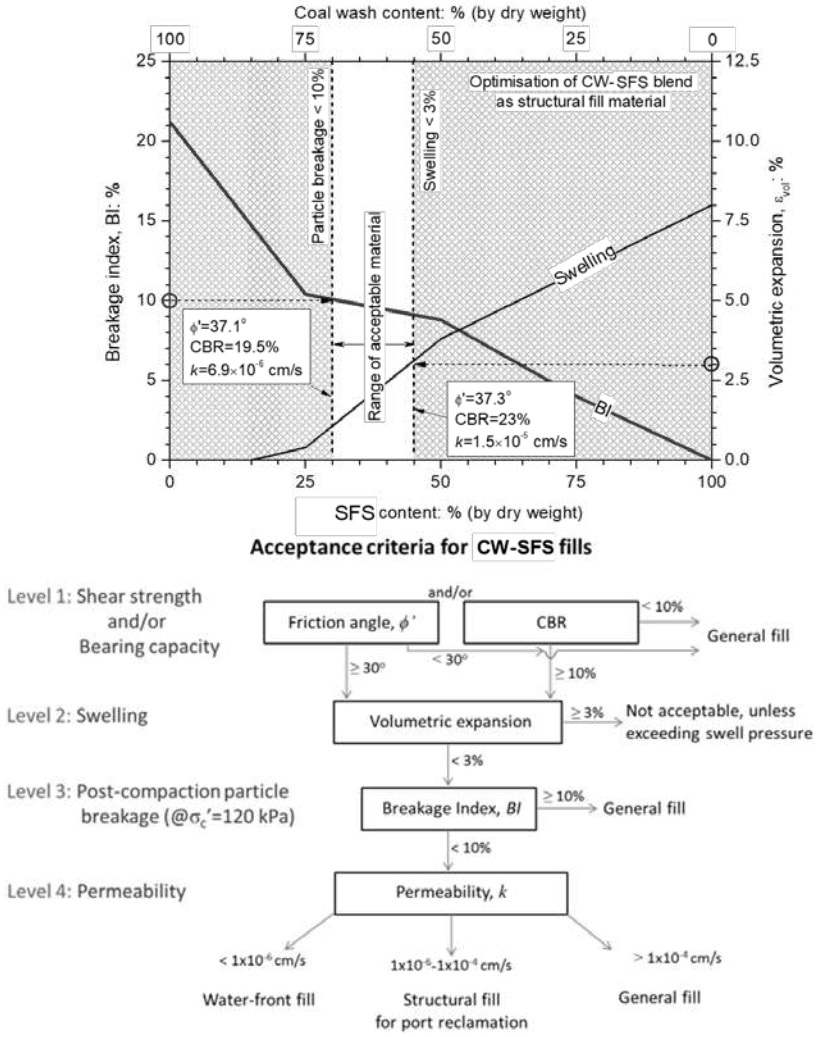

Figure 2. Criteria for defining the optimal CW-SFS blend (modified after Chiaro *et al.*, 2015).

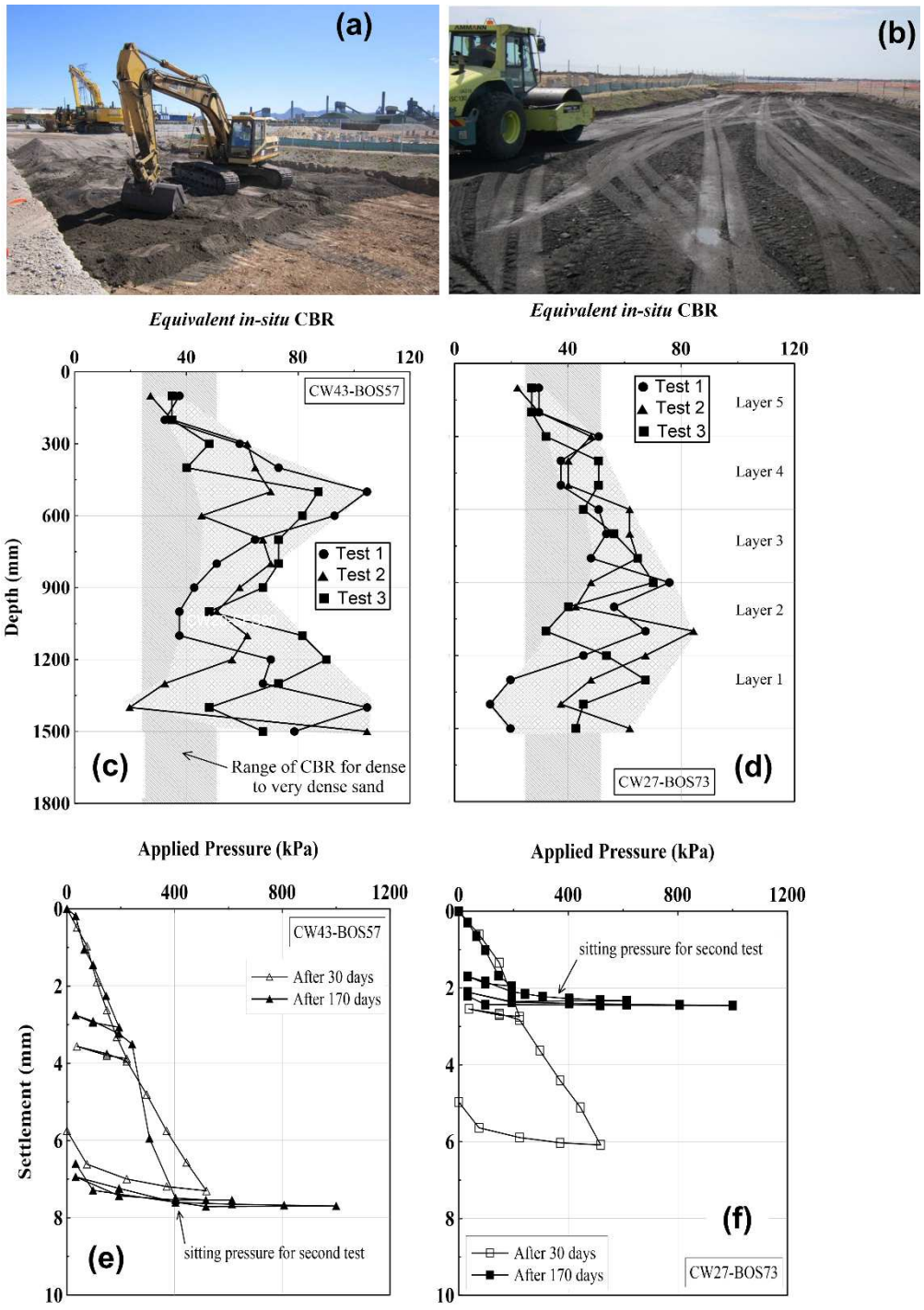

718

719 Figure 3. Photos of the field trial (a) spreading mixed materials, (b) compaction; (c-d) Variation of the
720 equivalent in-situ CBR with depth and (e-f) variation of pressure against settlement for CW50-BOS50 and
721 CW20-BOS80 (modified after Tasalloti *et al.*, 2015b).

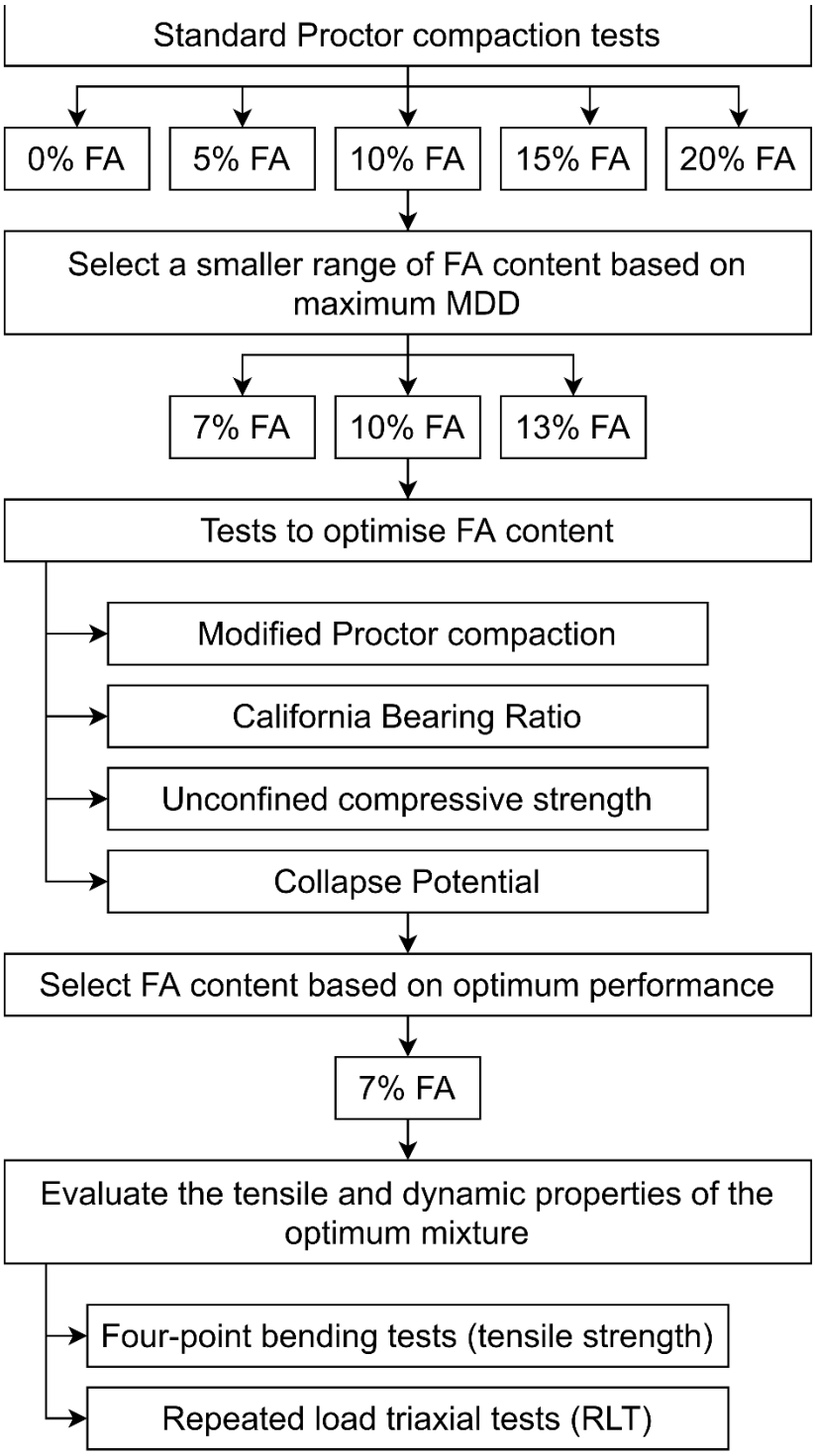

722

723 Figure 4. Experimental study for the optimization of a CW+FA mixture (modified after Wang *et al.* 2019).

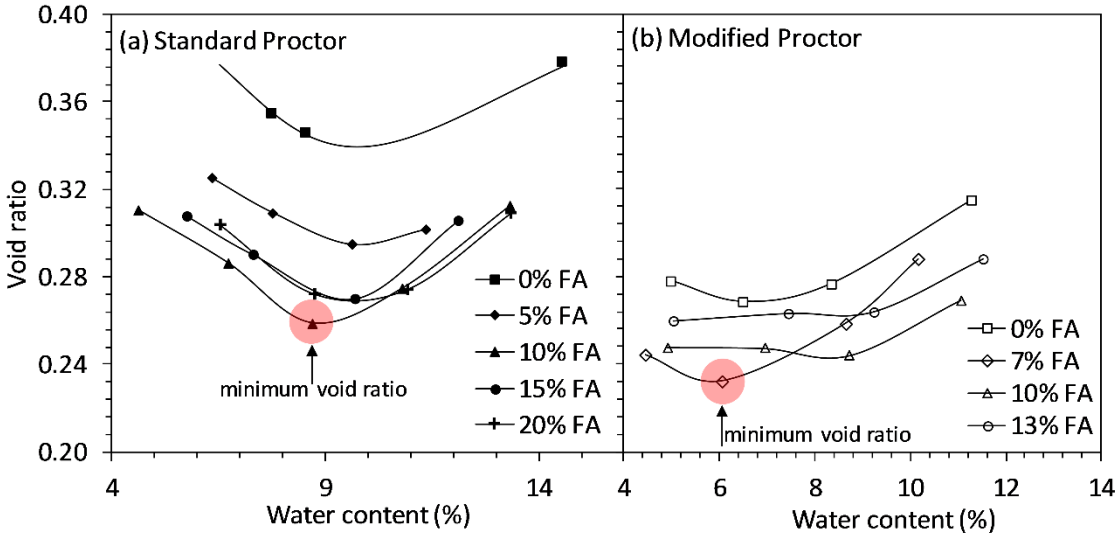

Figure 5. Compaction characteristics of CW+FA at (a) standard proctor and (b) modified Proctor.

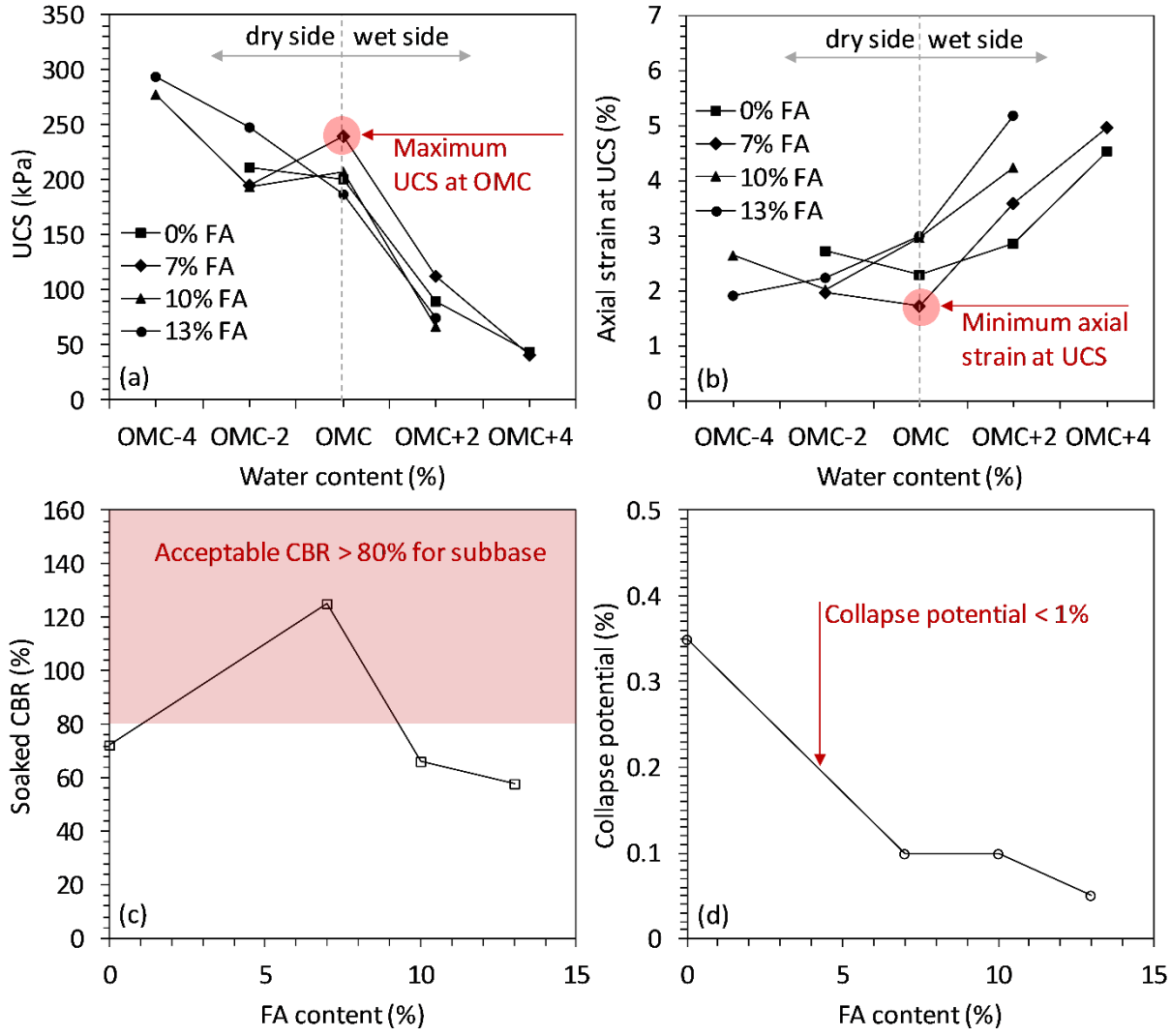

727

728 Figure 6. (a) Unconfined compressive strength, (b) maximum axial strain, (c) Soaked CBR and (d)

729 collapse potential of CW+FA mixtures (modified after Wang *et al.* 2019).

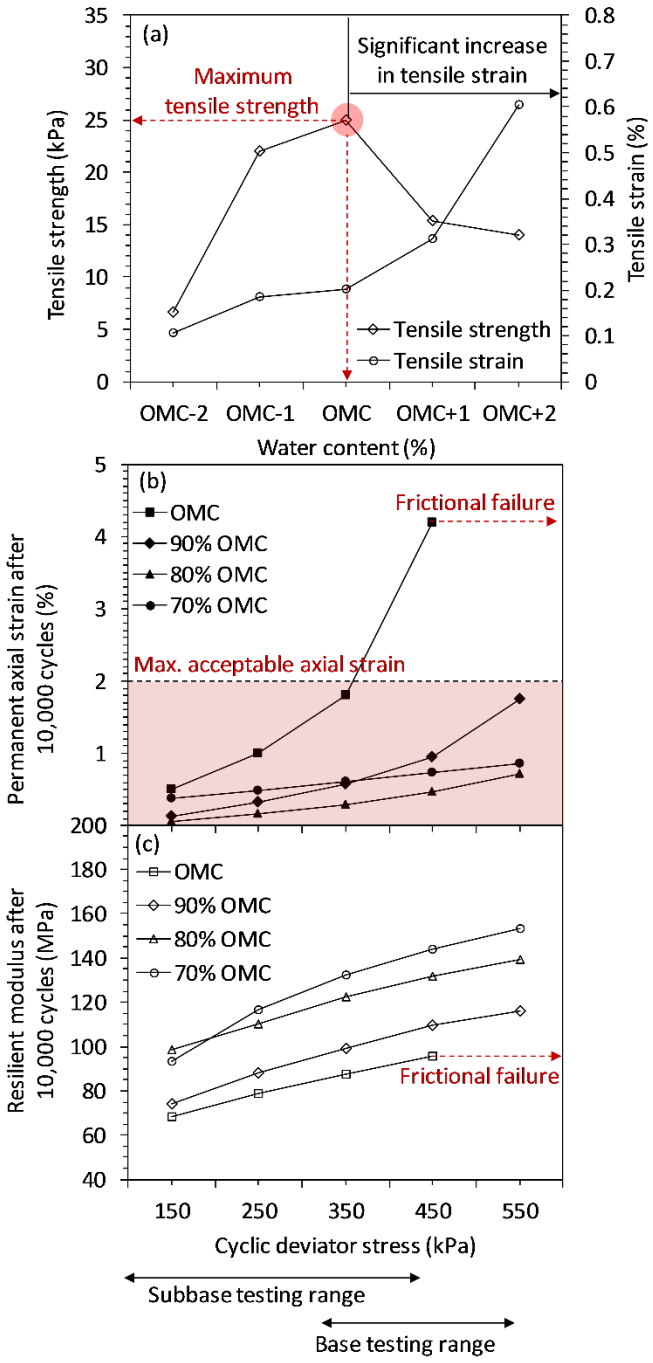

730

731 Figure 7. (a) Tensile strength, (b) Permanent deformation and (c) resilient modulus of CW+FA mixture

732 with 7% FA at different dry-back conditions.

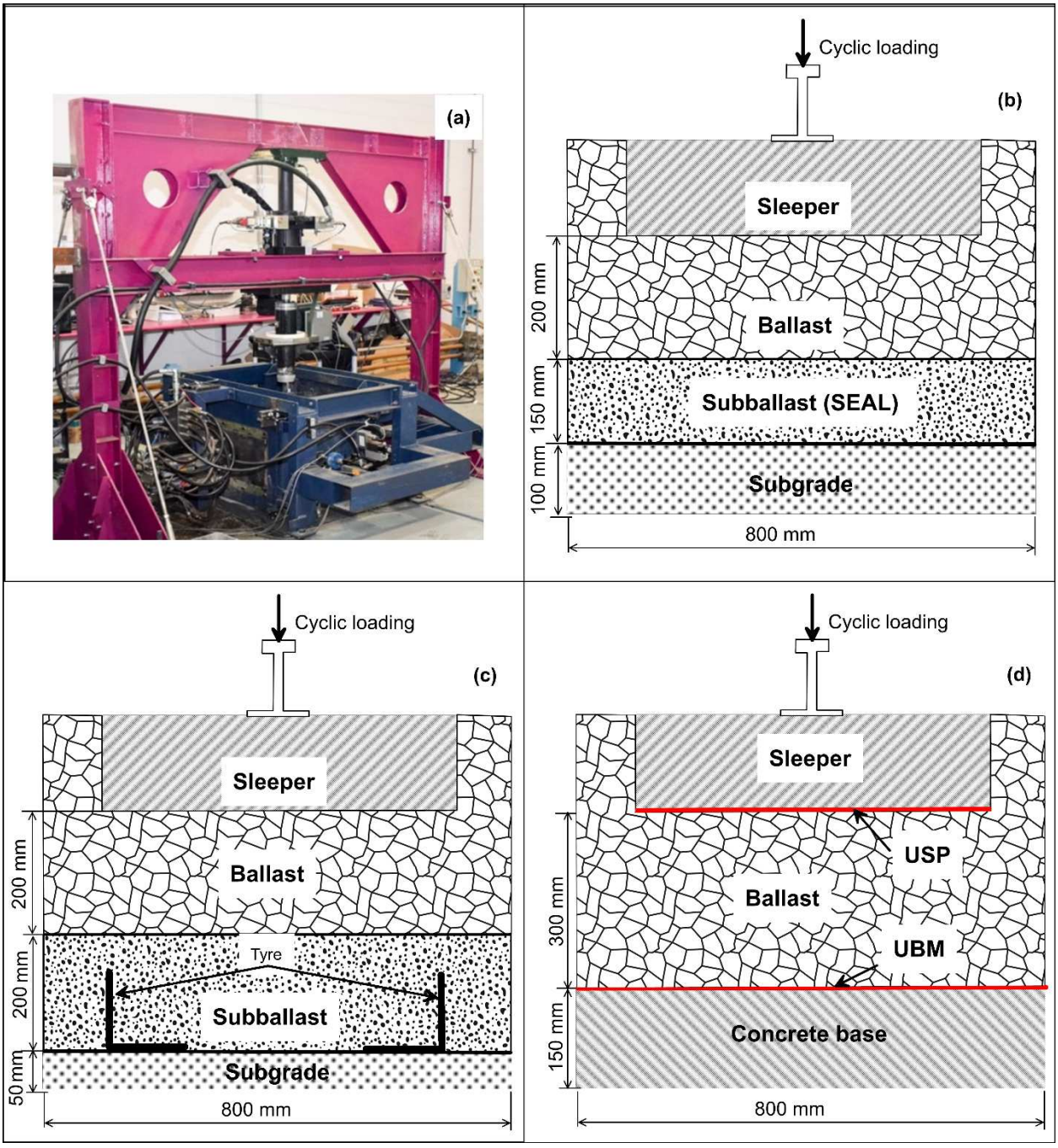

733

734 Figure 8. (a) Process simulation primordial testing apparatus (PSPTA) at the University of Wollongong,
735 and schematic illustration of (b) the physical model with SEAL, (c) the prismoidal triaxial box reinforced
736 with a recycled tyre cell, and (d) the prismoidal triaxial box with rubber mats.

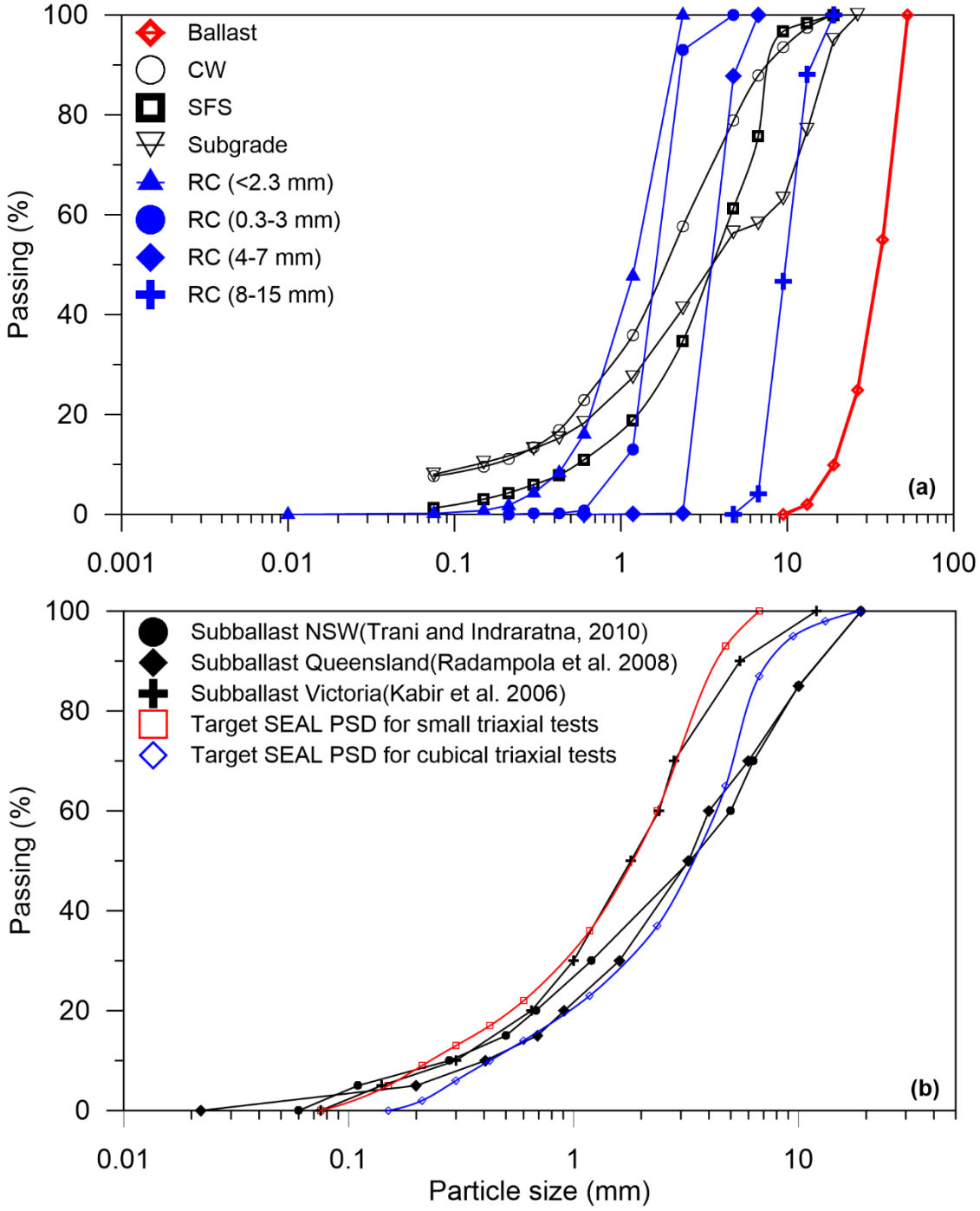

737

738 Figure 9. (a) PSD for ballast, subgrade, and waste materials; (b) PSD for traditional subballast and target

739 SEAL PSD for small and cubical triaxial tests.

740

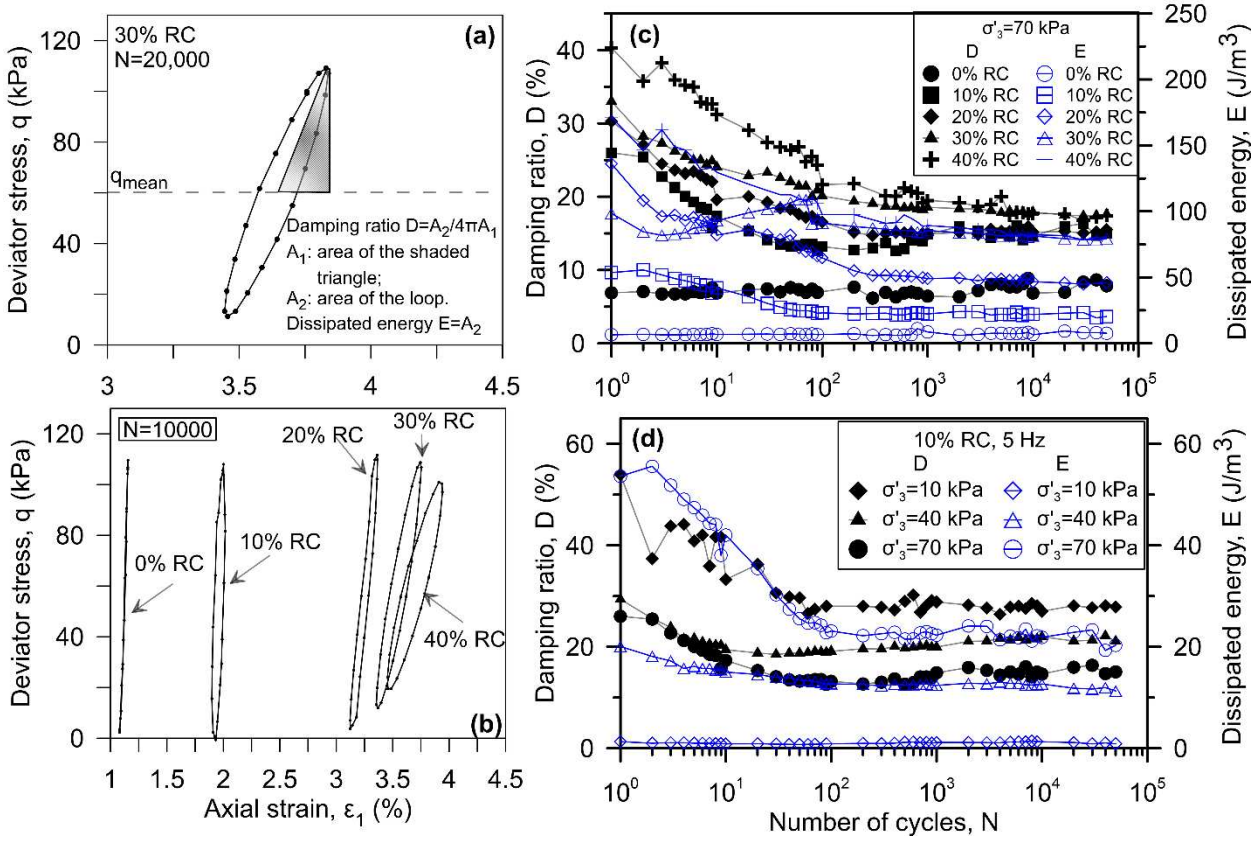

Figure 10. (a) Definition of damping ratio and dissipated energy; (b) hysteresis loops of the waste mixture having different RC contents, and damping ratio and dissipated energy of (c) SFS+CW+RC mixtures having different RC contents under $\sigma'_3 = 70\ kPa$, and (d) SFS+CW+RC mixtures having 10% RC under different σ'_3.

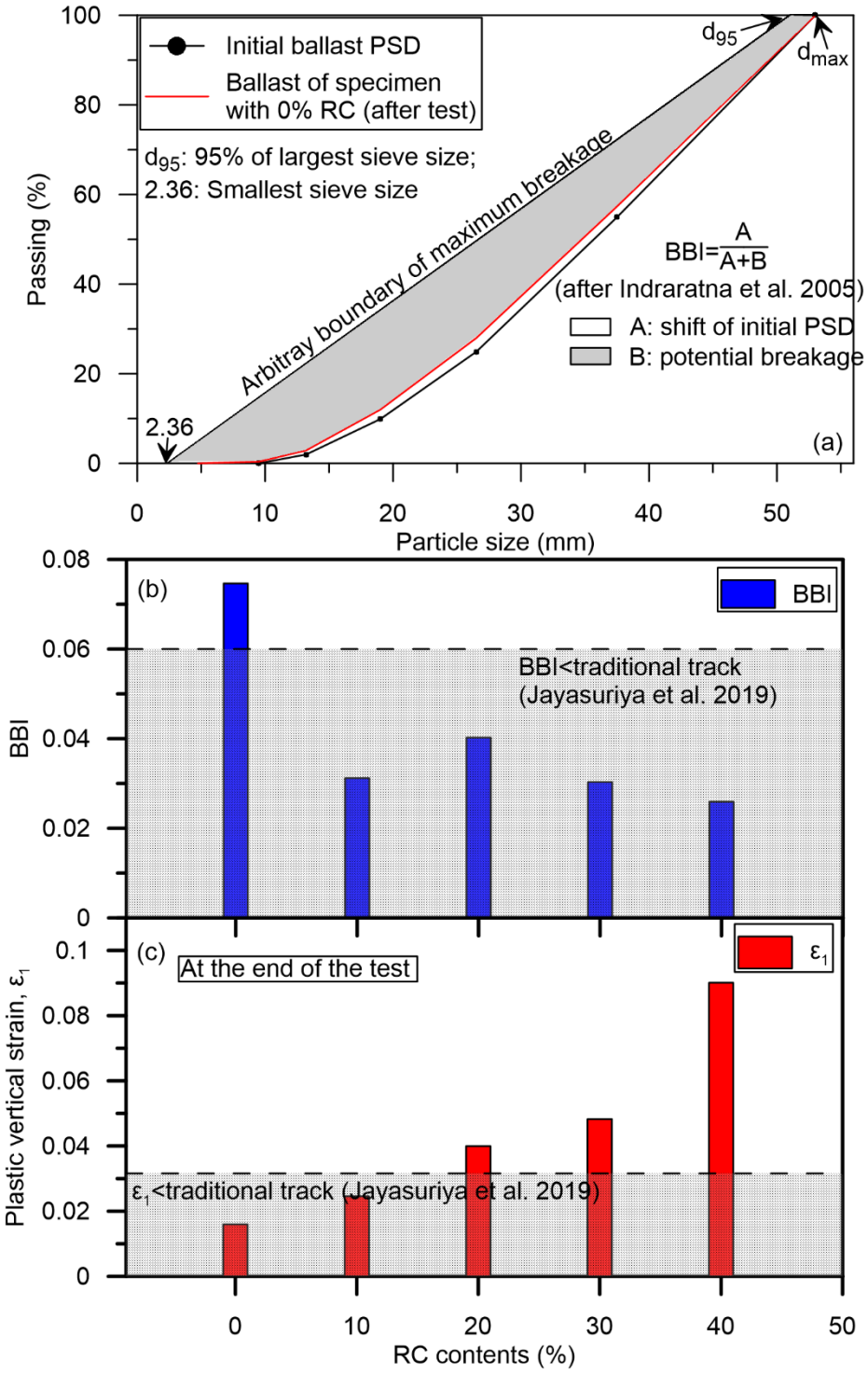

Figure 11. (a) Definition of BBI; cubical triaxial test result of (b) BBI and (c) plastic vertical strain.

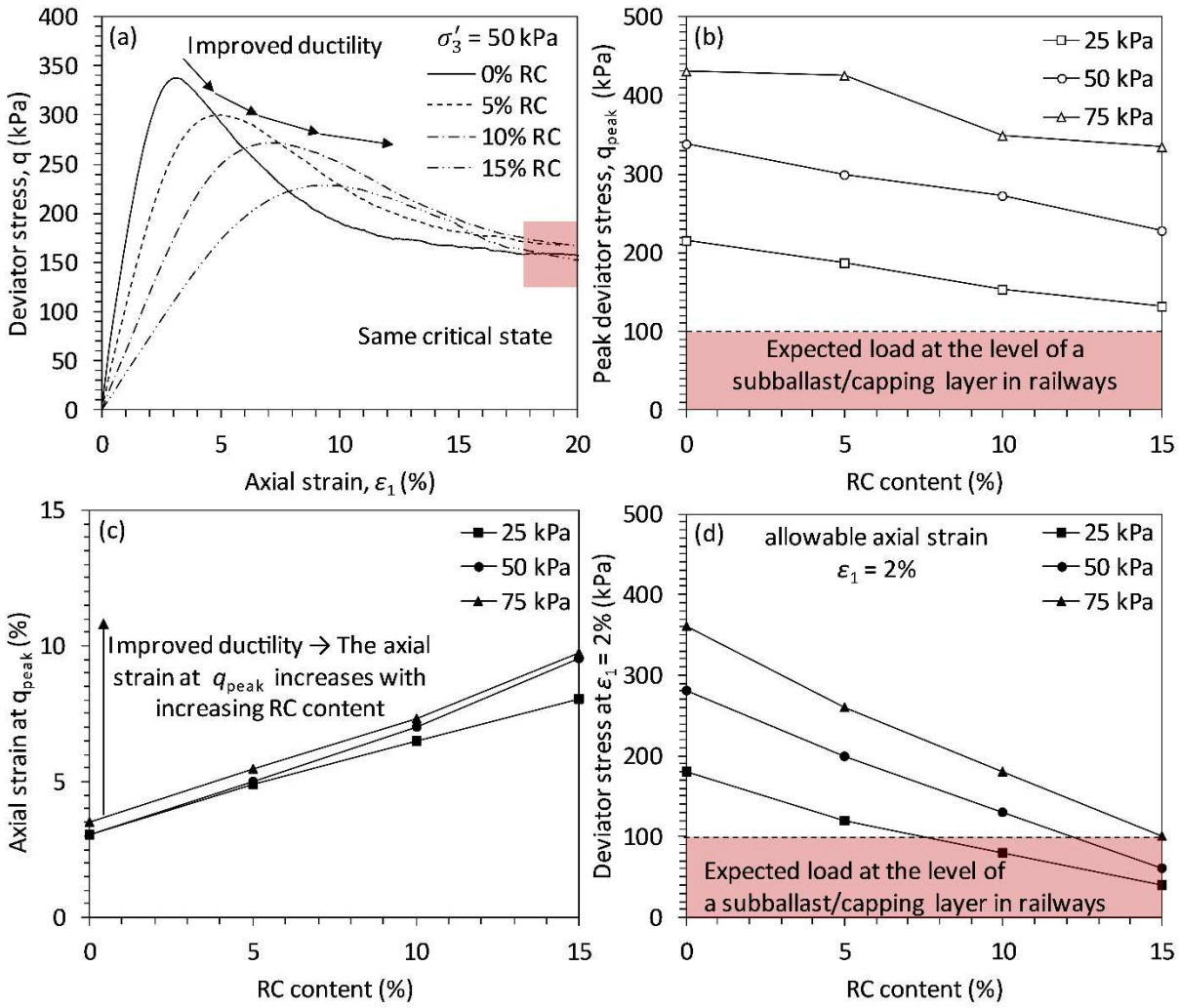

749

750

751 Figure 12. (a) Stress-strain curve at a confining pressure of 50 kPa and (b) peak deviator stress at

752 different confining pressures, (c) axial strain at q_{peak} and (d) q_{peak} at 2% axial strain of CW+RC mixtures.

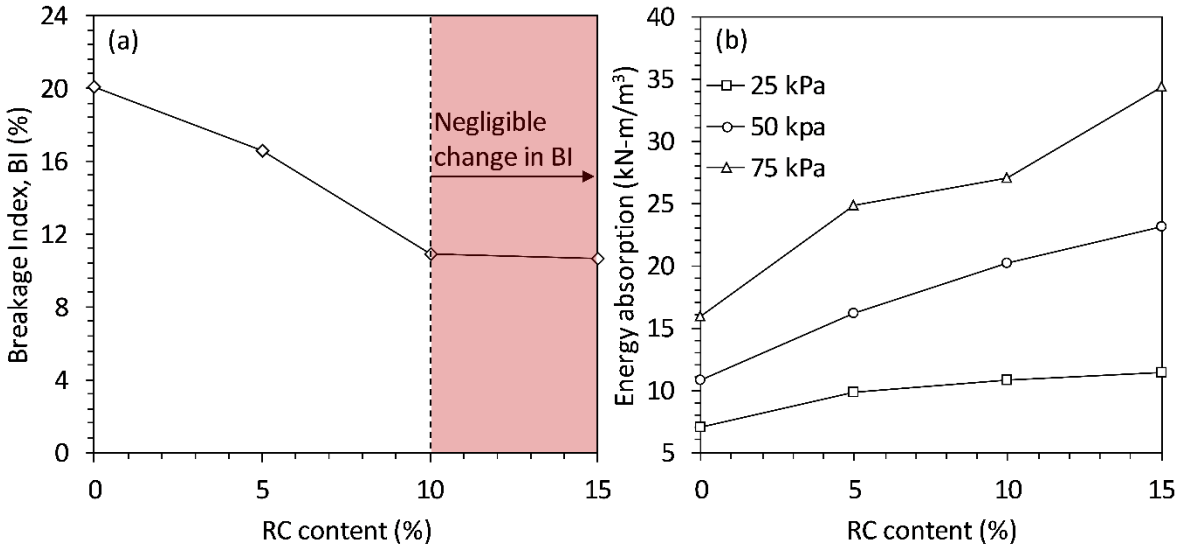

753

754 Figure 13. (a) Breakage Index (BI) and (b) energy absorption potential of CW+RC mixtures.

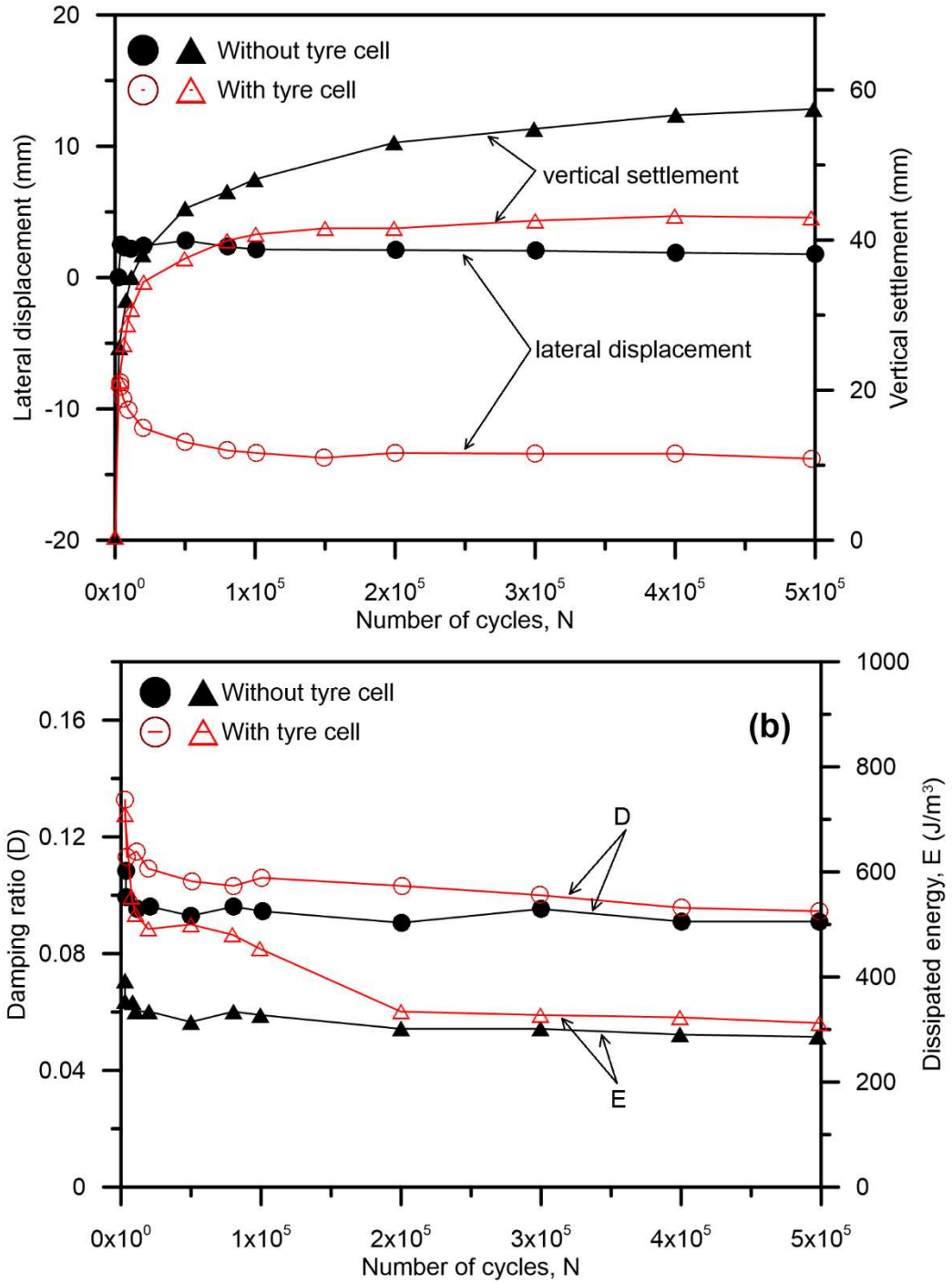

Figure 14. Cyclic cubical triaxial test results of the test specimen with and without tyre cell: (a) lateral displacement and settlement, and (b) damping ratio and dissipated energy (modified after Indraratna *et al.,* 2017c).

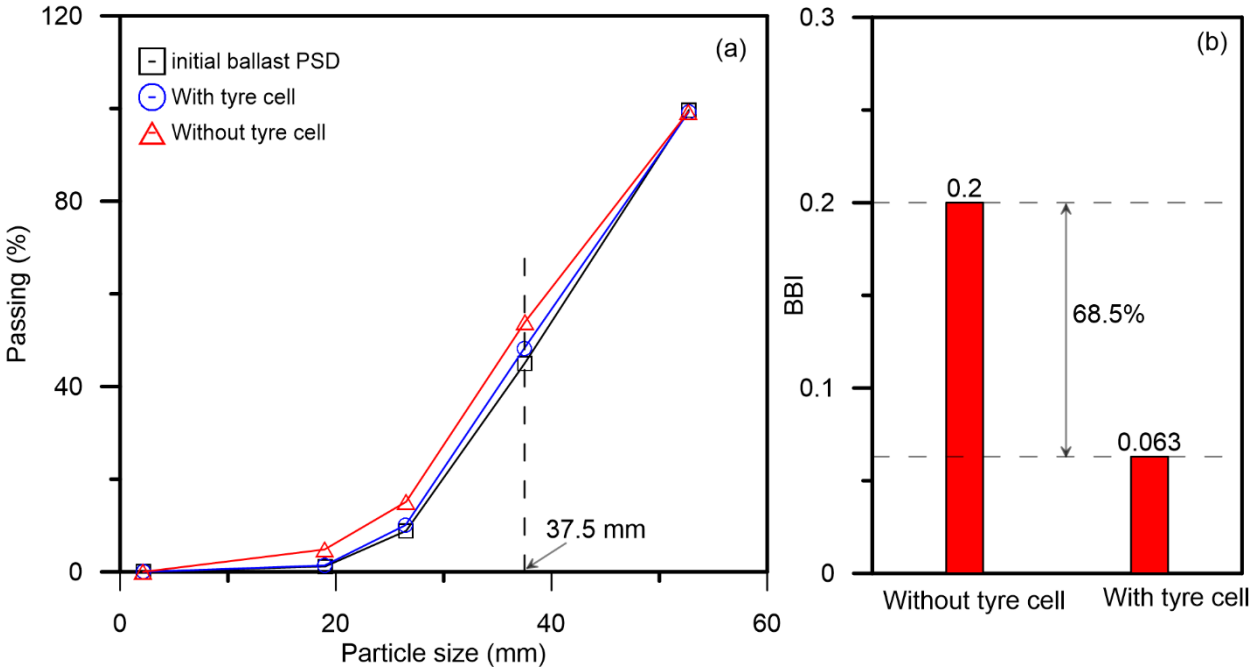

759

760 Figure 15. (a) The gradation of ballast before and after test; (b) BBI (data sourced from Indraratna *et al.,*

761 2017c).

762

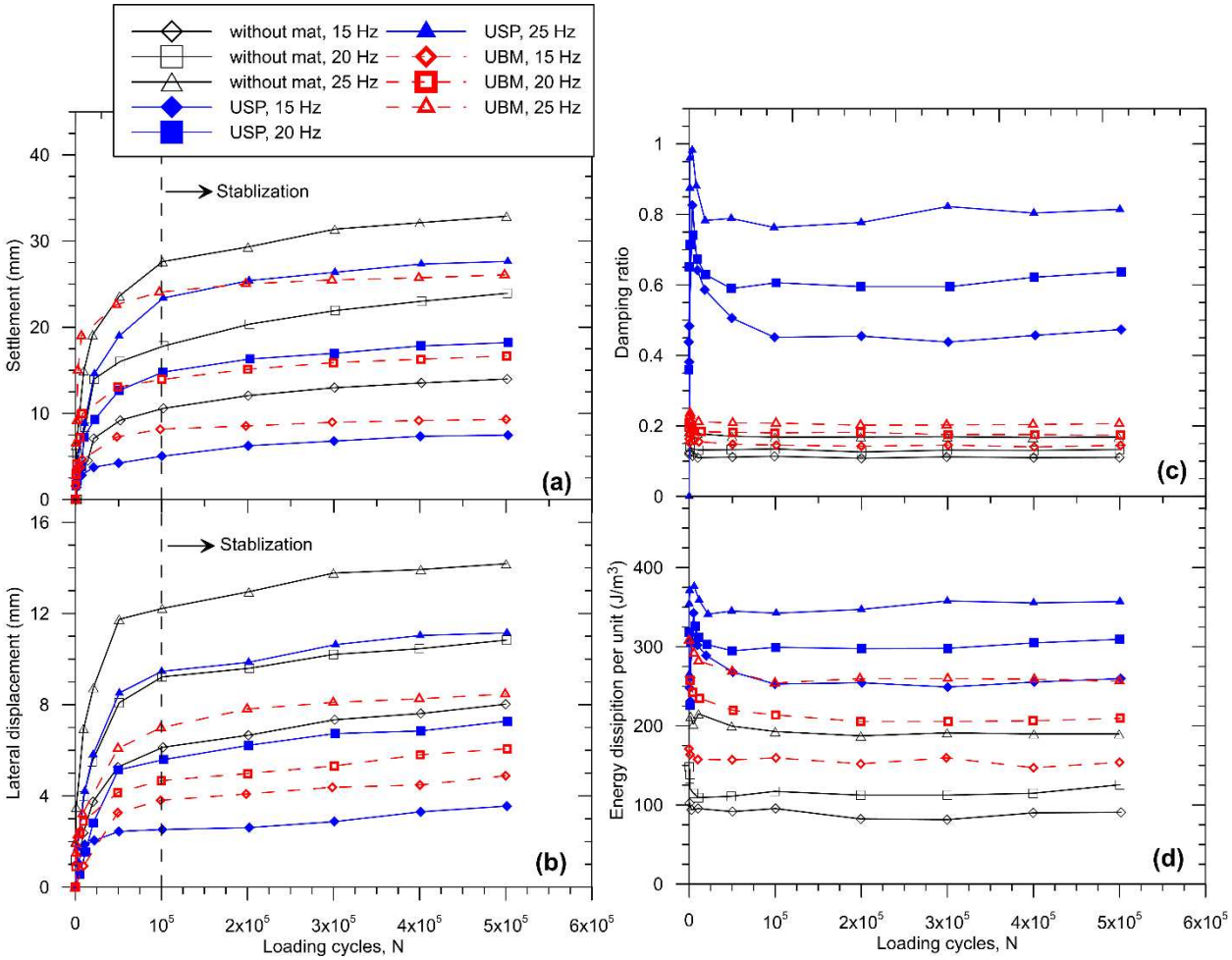

763

764 Figure 16. Cubical triaxial test results of the test specimen with USP or UBM or without rubber mats: (a)
765 settlement and (b) lateral displacement, (c) damping ratio, and (d) dissipated energy (data sourced from
766 Jayasuriya *et al.,* 2019 and Navaratnarajah and Indraratna, 2017).

767

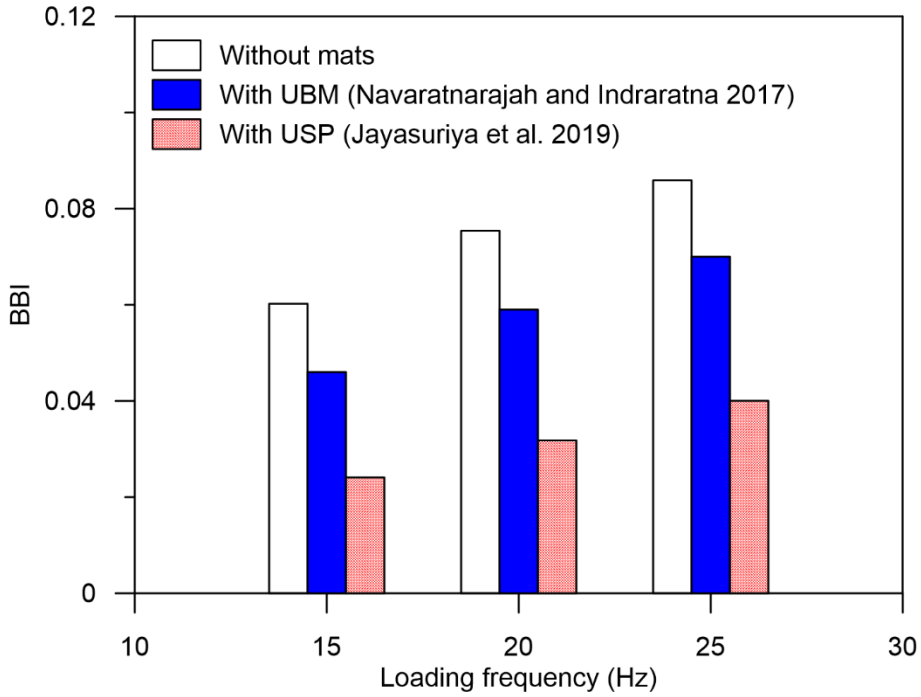

768

769 Figure 17. BBI of the test specimen with USP or UBM or without rubber mats.